830-D
NAS1.15:81868

NASA Technical Memorandum 81868

COMPLETED
58
ORIGINAL

Considerations for the Installation of Honeycomb and Screens To Reduce Wind-Tunnel Turbulence

James Scheiman

AUGUST 1981

NASA

NASA Technical Memorandum 81868

Considerations for the Installation of Honeycomb and Screens To Reduce Wind-Tunnel Turbulence

James Scheiman
Langley Research Center
Hampton, Virginia

NASA
National Aeronautics
and Space Administration

**Scientific and Technical
Information Branch**

1981

I

SUMMARY

Tests were conducted on a half-scale model representing a 0.914-m (3-ft) square stream tube of the flow through the fourth corner and settling chamber of the Langley 8-Foot Transonic Pressure Tunnel. The model included the finned-tube cooler, 45° turning vanes, and the turbulence reduction screens and honeycomb, which were the subject of the tests. Hot-wire measurements of the turbulence reduction for various combinations of screens and honeycomb were made at various duct speeds.

Of the four sizes of honeycomb cells tested, none were found to have a superior performance advantage. The effectiveness of screens and honeycomb in reducing turbulence is greatly affected by relatively minor physical damage; therefore, extreme care must be exercised in installing and maintaining honeycomb or screens if the turbulence reduction performance is to be maintained.

INTRODUCTION

The increasing cost of aircraft fuel makes it highly desirable for future aircraft to be more energy efficient. One approach to achieving this goal is to decrease aircraft drag. A major advance in decreasing drag would be obtained by maintaining laminar flow over the relatively large wing and tail surfaces. (See ref. 1.) In order to conduct laminar-flow research, a very low turbulence wind tunnel must be used. A study of a number of available wind-tunnel and flight test data was conducted to consider factors such as tunnel noise, Reynolds number, and turbulence level in flight (e.g., see ref. 2). This study concluded that the Langley 8-Foot Transonic Pressure Tunnel (TPT) was most suitable for conducting the laminar-flow experiments at high subsonic speeds.

Measurements in the 8-Foot TPT (refs. 3, 4, and 5) indicated that the flow disturbances were relatively low for a tunnel with no turbulence reduction devices; however, the tunnel required modifications to reduce the test-section turbulence to even lower levels to permit laminar-flow tests. Screens and honeycombs have been used extensively in other tunnels as flow straighteners and for turbulence reduction. Introducing these flow manipulators into the flow stream increases the required power because of the additional flow resistance (pressure drop) in moving the fluid through the manipulators. Since the pressure loss is proportional to the mean speed of the fluid flow, the manipulators are generally installed in the low-speed portion of the wind tunnel, downstream of the last major turbulence generators ahead of the test section. In the 8-Foot TPT, this is the section between the cooler and the contraction (fig. 1), where there seems to be adequate length for several turbulence reduction devices. Because of the scarcity of literature applicable to the 8-foot tunnel, a half-scale model of a stream tube of the tunnel, without the contraction, was fabricated (fig. 2) for tests to evaluate the effectiveness of various devices.

Screens of six different mesh sizes and honeycomb of four different cell sizes were evaluated. Various combinations of these manipulators were tested to determine their effectiveness in reducing the turbulence levels. Conventional hot-wire probes were used to measure the axial and lateral turbulence. Acoustic microphones were used to monitor the operational noise generated in the model duct. The test speed varied between 7.62 and 18.29 m/sec (25 and 60 ft/sec). Over 250 configurations were examined; however, only a small portion of the data are presented. A few important experiences and conclusions are also presented. The selection of a configuration for incorporation into the 8-Foot TPT is not discussed herein but is presented in reference 6. Additional data concerning correlation of experiment with theory are presented in reference 7. It is important to keep in mind that the conclusions presented are applicable primarily to the Langley 8-Foot Transonic Pressure Tunnel with its unusual configuration of finned-tube cooler and turning vanes.

Identification of commercial products in this report is used to adequately describe the model. The identification of these commercial products does not constitute official endorsement, expressed or implied, of such products or manufacturers by the National Aeronautics and Space Administration.

SYMBOLS

d	diameter of cooler tube, cm (in.)
e'	rms voltage divided by mean (dc) voltage × 100, percent
E	mean (dc) volts, V
f	Strouhal shedding frequency, Hz
ℓ	model duct length (10.5 m (34.5 ft))
L_{jk}	hot-wire calibration constants (see eqs. (3) in appendix)
m	fluid mass-flow rate, kg/s
P	pitch angle of fluid flow sensor (see fig. 7), deg
S_i, S_{ij}	hot-wire calibration constants (see appendix)
S_t	Strouhal number used in table III
u'	rms axial velocity fluctuations, nondimensionalized by dividing by mean flow velocity and multiplying by 100, percent
U	free-stream velocity, m/sec (ft/sec)
v'	rms lateral velocity fluctuation, nondimensionalized by dividing by mean flow velocity and multiplying by 100, percent
Y	yaw angle of fluid flow sensor (see fig. 7), deg

σ standard deviation of hot-wire data

θ angle of fluid flow with respect to normal to axis of hot-wire probe (see appendix), rad

Subscripts:

i denotes component of turbulence; 1 for u', 2 for v'

j 2 or 3 denotes one wire of cross-wire probe

k 1 denotes slope of equations (3); 2 denotes intercept of equations (3)

NOM nominal value

ref reference value

Abbreviations:

1/16 HC, 1/8 HC, 1/4 HC, etc. designate various sizes of honeycomb cell used (see table II)

8M, 20M, 28M, etc. designate various sizes of screen mesh used (see table II)

rms root mean square

DISCUSSION OF APPARATUS AND TECHNIQUES

Model

A drawing of the Langley 8-Foot Transonic Pressure Tunnel is shown in figure 1. To decrease the turbulence in the tunnel test section, turbulence manipulators could be inserted between the turning vanes (downstream of the cooler) and the contraction sections. As seen in the figure, the limited available axial lengths on the inside portion of the turn posed a major problem for insertion of the manipulators. To evaluate the effectiveness of various manipulators, a half-scale model was fabricated of a stream tube through the center of the corner and the settling chamber where the manipulators could be inserted. A contraction was not included. The scale of the model was dictated by two factors. The first was the availability of existing duct components and drive system. (See ref. 8.) The second was the availability of reduced-size finned tubes to represent the cooler. These two factors favored a half-scale model. A dimensional comparison of the actual and scale-model coolers is presented in table I. The available ducting had a cross section 46.36 cm (18.25 in.) square. Therefore, sufficient cooler tubes and turning vanes were fabricated to fill the model test section.

Eight staggered rows of half-scale cooling tubes were used to duplicate the finned-tube cooler of the full-scale tunnel. Since most of the manipulator configurations evaluated had the manipulators installed normal to the flow, the

distance between the turning vane and the first manipulator varied across the duct section, as seen in figure 1. Therefore, spacers for the half-scale model were fabricated to simulate the full-scale tunnel centerline and a section 4.57 m (15 ft) on either side of the centerline. Time limitations permitted the testing of the centerline configuration only. A sketch of the half-scale test model is shown in figure 2. Photographs of the test model and the upstream portion of the cooling tubes are shown in figures 3(a) and 3(b), respectively.

From figure 1, it can be seen that the first 45° of the turning occur through the cooler and the second 45° occur through the turning vanes (45° turning vanes). After some discussion, it was concluded that, because of the relatively high pressure loss across the cooler, there was probably more air passing through the outer radius of the turn of the cooler than through the inner radius. Further, the air entering the cooler probably varies across the duct section. Therefore, the model simulation of this portion of the duct (actual tunnel centerline) should aid the fluid in turning into the cooler. This fairing is shown sketched in figure 2.

The dimensions of the screens chosen for evaluation are presented in table II. The various mesh sizes were chosen to cover a wide range. A major consideration was the screen percent open area which must be kept subcritical (ref. 9), at least 58 percent open.

The screens were permanently mounted in square frames, with a frame thickness equal to between 80 and 100 screen mesh sizes. The data in reference 10 indicate that almost all of the turbulence decay occurs within 50 to 75 screen mesh sizes downstream of the screen. Therefore, whenever multiple screens were being evaluated, the corresponding frame thickness provided assurance that turbulence was adequately decayed before the air encountered the next manipulator.

The honeycomb characteristics chosen for evaluation are also presented in table II. These configurations were chosen based on information in reference 10 and on personal consultation with one of the authors, Dr. Hassan M. Nagib. The honeycomb material was aluminum or stainless steel. One primary criterion was that the honeycomb cell length-to-cell-size ratio be between 6 and 8.

In general, the honeycomb was installed in the duct at the farthest upstream position of the manipulator section and the first following screen was positioned 0.3 m (1 ft) downstream of the downstream end of the honeycomb. (See fig. 2.) (Exceptions occur when evaluating the 45° honeycomb or when the screen is in direct contact with the honeycomb, then this honeycomb-screen combination is installed in the farthest upstream position.) The turbulence decay data in reference 10 indicate almost complete decay within 23 to 25 cm (9 to 10 in.) downstream of the simulated honeycomb, made of soda straws. This distance corresponds to about 50 soda-straw diameters or between 1 to 10 cell-depth dimensions. For the tests herein, the 0.3-m (1-ft) spacing corresponds to 32 to 200 cell diameters or 4.5 to 28 cell-depth dimensions, respectively, for the 3/8- to 1/16-cell size honeycomb. Therefore, except for the noted exceptions, the data presented herein for the honeycomb-screen combinations indicate that the turbulence from the upstream honeycomb is almost completely decayed before encountering the first screen.

Instrumentation and Data Reduction

The instrumentation system used varied during the test program. Both static (mean velocities and pressure) and dynamic flow measurements were made. Two, duplicate pitot-tube systems were installed at the farthest downstream instrumentation cross section of the model. (See fig. 2(b).) These sensors were connected to long sections of pressure tubing (over 3 m (10 ft) long) which were in turn connected to pressure transducers and digital voltmeters. This system was used to measure the duct velocity, which was the reference velocity, and was not changed during the entire test. Initially, a total pressure rake and static-pressure tapes along the wall were used to measure the flow characteristics of the duct between the turning vane and the instrumentation section. This survey was conducted using a cross rake connected to three electrically actuated pressure scanning valves with pressure transducers.

An accelerometer was used during various portions of the test. This sensor was used to detect duct-wall and hot-wire support system vibrations to assure that the hot-wire output did originate from fluid turbulence rather than support vibrations.

Three channels of the hot-wire electronic system were manufactured by DISA Electronics, division of DISAMATIC, Inc. (DISA) and two channels by TSI Incorporated (TSI). Except for the initial preliminary testing, the hot wires had fixed locations during the test. One of the DISA hot-wire channels was used for a one-wire probe and the other two channels were used for a cross- or x-wire probe. With only one exception, the single-wire probe was 2.54 cm (1.00 in.) off the duct centerline and the cross-wire probe was 2.54 cm (1.00 in.) off the centerline in the opposite direction (thus, the two sensors were 5.10 cm (2.00 in.) apart). These three wires were also located in a plane that was 30 cm (12 in.) downstream of the last manipulator and approximately 53 cm (21 in.) upstream of the pitot tubes. (See fig. 2(b).)

The TSI hot-wire electronics channels were used for single wires only. In general, these two hot wires had fixed locations during the testing. They were located in the duct approximately 12.70 cm (5.00 in.) from the wall. One wire was in a plane approximately 1.58 m (5.19 ft) downstream of the center of a line through the trailing edge of the turning vanes. The second wire was approximately 2.55 m (8.36 ft) downstream of the same centerline point. These two separate wires were both upstream of the manipulators and were thus used to assure that the turbulence going into the manipulators had a relatively constant value. A schematic diagram of the hot-wire instrumentation system is shown in figure 4.

Two, standard, half-inch condenser microphone systems were used during the entire testing. Both of these systems had microphones flush mounted in the wall of the duct and isolated from wall vibrations. One microphone was mounted approximately 0.41 m (1.3 ft) downstream of the center of the line through the trailing edge of the turning vanes, and the other microphone was in the plane of the pitot tubes, near the downstream end of the instrumentation section. These microphones were used to detect any acoustic waves traveling up or down the duct.

Such acoustic waves would be detected in the output of the hot wires and could be misinterpreted as turbulence.

All hot-wire and acoustic data were recorded on a frequency modulated (FM) tape recorder. The digital voltmeter used to measure the output from the pitot gages were manually read and recorded. The hot-wire voltages were monitored on an oscilloscope, and the output voltages were manually read and recorded before recording on the tape recorder. Standard hot-wire data reduction equations were used and, for completeness, they are presented in the appendix.

Assessment and Development of Apparatus and Test Procedures

The program developed as it progressed, mainly because of numerous difficulties that were encountered in obtaining valid results. These problems influence the results of the investigation and may be of interest to subsequent investigations. Hence they are discussed in some detail herein.

Model tunnel flow survey.- Since the half-scale tunnel model represents a small, cross-sectional stream-tube area of the full-scale tunnel, there was some concern about possible effects of the boundary-layer "build up" on the walls of the model. Recall that the cross section of the model tunnel was 46.36 cm (18.25 in.) square, and the distance between the 45° turning vanes and the first manipulator is approximately 3.1 m (10.0 ft). In response to this concern, a survey of the mean flow velocity was conducted in the model tunnel using a pitot-tube rake. A portion of the rake survey data results are shown in figures 5 and 6. Presented in figure 5 are the results of a vertical and lateral survey at a position 0.42 m (1.42 ft) downstream of the centerline of the trailing edge of the 45° turning vanes. The various reference speeds were determined by the reference pitot tube. (See fig. 2(b).) The vertical velocity distribution (fig. 5(a)) seems to be fairly uniform, especially at the higher mean speeds where the accuracy of the instrumentation is greater. Some of the scatter in the data is due to difficulties in making accurate pressure measurements at the low speeds. The lateral velocity distribution (fig. 5(b)) seems to have about the same variation as the vertical distribution survey. In the right side of figure 5(b), the horizontal location of the trailing edge of the 45° turning vanes is marked by arrows. At some of the mean duct speeds, the velocity variations indicate the vane wakes, which seem to correlate with the vane-trailing-edge locations. A slight increase in velocity on the outer edge of the duct turn is also indicated in figure 5(b).

Presented in figure 6 are the results of the velocity survey at varying distances downstream for one constant mean velocity. Figures 6(a) and 6(b) are plots of the vertical and lateral velocity distributions, respectively. This figure indicates that the flow leaving the 45° turning vane seems to become more uniform as it moves downstream. Further, this figure clearly shows the increasing boundary-layer thickness with increasing distances downstream. The boundary layer appears to be between 2.54 and 5.10 cm (1.00 and 2.00 in.) thick at the manipulator installation locations, but the center portion of the duct is clearly usable for making the turbulence measurements.

Comparison of model tunnel with full-scale tunnel.- After the half-scale model was assembled and before valid manipulator-turbulence-reduction tests could be conducted, numerous tests were required to compare the model results with the full-scale tunnel results. In the full-scale tunnel, turbulence and mean-velocity measurements were made upstream of the cooler, between the cooler and the 45° turning vanes, and in the contraction sections. (See fig. 1.) Some of these results are reported in references 3, 4, and 5. Dynamic flow measurements were made using a flow-direction and speed sensor described in reference 11 which can respond to frequencies up to perhaps 20 Hz. The flow-direction (pitch and yaw) measurements as a function of time are shown in figure 7 for three wind-tunnel Mach numbers. The data indicate that the flow direction upstream of the cooler was very unsteady, with approximate flow angularity variations of ±20°. The speed variations ahead of the cooler were also very unsteady. The frequencies of these variations were quite high, and it was concluded that the dynamic response of the sensor was limiting the resulting sensor output. Attempts were made to simulate the disturbance upstream of the cooler in the half-scale model. Fortunately, the extreme techniques that were tried (i.e., airfoil vanes and cylinder vortex generators) resulted in very small differences in turbulence downstream of the cooler. It was concluded that the cooler performed as a very good fluid damper and flow straightener. For flow downstream of the cooler, it can be seen in figure 7 that this was indeed true. Although the flow-angle measurements in figure 7 have not been corrected for the sensor orientation, it can be seen that the flow exits normal to the cooler and parallel to the tunnel walls at the turning vanes. (See fig. 1.) The turning vanes are actually constructed to overturn the flow by 2.5°. The mean flow speed between the cooler and the 45° turning vanes was about 6.86 m/sec (22.5 ft/sec), and the speed downstream of the 45° turning vanes normal to the circular-duct axis was about 8.5 m/sec (28.0 ft/sec). These speeds were approximately the same for tunnel test-section Mach numbers between 0.75 and 0.84.

The pressure loss across the model and full-scale coolers was measured and found to compare favorably. The ratio of the measured cooler pressure loss to the dynamic pressure was about 6.5.

The full-scale-tunnel turbulence measurements (refs. 3, 4, and 5) upstream of the cooler indicate high turbulence levels. The axial turbulence levels downstream of the cooler and 45° turning vanes (in the settling chamber) were about 2 percent in the full-scale tunnel. The measured model results matched very closely the full-scale results, thus verifying the turbulence level of the cooler and turning vane model.

Speed range and test procedure.- The test speeds were dictated by scaling laws. Reynolds number scaling based on cooler tube diameter (ratio of dynamic fluid forces to viscous fluid forces) requires doubling the speed for the half-scale model to keep the same Reynolds number. Strouhal frequency scaling requires halving the speed for the half-scale model to keep the same shedding frequencies. The mean speed in the plenum of the full-scale tunnel ranged from about 4.6 to 9.1 m/sec (15.0 to 30.0 ft/sec), and the model test speeds ranged from 7.6 to 21.3 m/sec (25.0 to 70.0 ft/sec).

Each test configuration was evaluated by installing the manipulators, sealing the duct, and conducting the tests over the speed range. At each test speed, the hot-wire rms and dc voltages and the duct operating conditions were manually read and recorded. The hot-wire and acoustic data were then recorded on FM tape for more extensive data reduction and analysis. An on-line spectra analyzer and correlator were used periodically to review particular conditions. After the speed range was completed, the manually recorded data were immediately analyzed for a preliminary evaluation. Some suspect data points were repeated before proceeding to the next manipulator configuration. Approximately 250 manipulator configurations were evaluated.

Air-drive system.- A conventional hot-wire sensor system does not separate acoustic waves from vorticity (fluid turbulence). Screens and honeycombs primarily modify fluid turbulence and have little effect on acoustic waves. Since the object of the present program was the reduction of fluid turbulence, acoustic noise was considered undesirable interference. As the turbulence level is decreased, the significance of the acoustic interference increases. The original fan drive system of the model, which is not shown in figure 2, was a major acoustic noise source, since it was located very close behind the instrumentation section and had to produce sufficient pressure rise to overcome the pressure loss through the cooler and a multitude of manipulators. The fan had been designed for other investigations to operate with large mass flows and with a relatively low pressure rise, but in the present tests with the cooler and screens, it was required to operate at low mass flows and high pressure rise. This off-design fan operation was very noisy.

The first 400 test runs were conducted using this axial-flow fan mounted a few feet downstream of the reference pitot tubes. Numerous techniques were attempted to overcome the noise problem, including taking the arithmetic difference between the turbulence measurements with and without the manipulators present with the drive fan operating at the same load conditions. Such attempts to overcome noise problems were unsuccessful, and finally, a different drive system was incorporated. The new drive system location is shown schematically in figure 2.

This new air-drive system consisted of three tip-driven-turbine air motors that operated at very high rotational speeds, namely 8000 to 20 000 revolutions per minute. These motors were enclosed in an acoustically lined box with various internal baffles to keep the air-motor-generated noise from moving up the diffuser and contaminating the hot-wire measurements. The acoustic box was very effective in reducing the air-drive-motor noise. However, as the turbulence level was reduced, other noise sources became noticeable, but at a lower noise level (e.g., the noise from the air passing through the cooler). Presented in table III(a) are the frequencies that have been identified as originating from the cooler. As expected, these frequencies vary directly with speed (Strouhal eddy shedding). The two microphones placed along the duct were cross correlated to determine the direction of travel of the acoustic waves. For example, diffuser separation noise was identified as another noise source; and vortex generators installed in the diffuser attenuated this noise source. Each reduction in the noise level resulted in a new, lower noise (or hot-wire-measured turbulence) floor.

One other acoustic source was identified that might be of interest, the standing waves within the duct itself. Under some operating conditions (speed and manipulator combinations), these standing waves could be excited. Presented in table III(b) are some natural acoustic frequencies and hot-wire frequencies that did not vary with duct speed. The length of the duct from the cooler to the acoustic box is approximately 10.5 m (34.5 ft). This length corresponds to the frequencies presented in table III(b) and was used to calculate the air column frequencies. By incorporating a 100-Hz high-pass filter to the hot-wire data acquisition system, the effects of the standing waves could be effectively eliminated. Initially, turbulence data were recorded at different high-pass-filter settings, namely 2 Hz, 10 Hz, and 100 Hz. In general, it was found that the relative turbulence reduction (with the same filter) was approximately the same for the various manipulators. Therefore, all data reported for runs after number 564 are for the 100-Hz high-pass filter.

Initially, the low-pass filter was set at 10 kHz. A review of the spectra indicated that most of the hot-wire information had frequencies below about 3 kHz. Therefore for runs after number 679, the low-pass filter was set at 5 kHz.

Hot-Wire Measuring Accuracy

It is difficult to make accurate hot-wire measurements and even more difficult when the turbulence levels are very low. However, in order to validate both the turbulence data presented and the conclusions reached, some estimate of accuracy must be attempted.

To evaluate the accuracy of the hot-wire data, the data reduction equations were reviewed. (See appendix.) This review indicated that a direct evaluation of the sensitivity of the input parameters was not possible. Therefore, mean values of all the input variables were chosen. Then an arbitrary ±10-percent error in each variable was introduced, one variable at a time, into the data reduction equations. The results are shown in figure 8. Shown in figure 8(a) are the resulting errors in axial and lateral turbulence for input error in the measured voltages. Shown in figure 8(b) are the errors for input errors in the hot-wire calibration constants. The results show the nominal (mean) value of turbulence and the ±10-percent error range. The figures show that the axial-turbulence (u') accuracy stays within the ±10-percent band, whereas the lateral-turbulence (v') errors can be much larger than ±10 percent. The data reduction equations indicate that errors in measurement with the cross-wire probe will not affect the axial turbulence, but errors in the single-wire measurements will affect the lateral turbulence. In other words, it will be more difficult to obtain accurate lateral turbulence than axial turbulence.

A further assessment of the accuracy was made as follows. Recall that one hot wire (a single wire) was placed between the 45° turning vanes and the first manipulator. (This wire was used to assure that the turbulence leaving the turn and/or entering the manipulators was relatively constant.) The measured output from this wire was tabulated over a 30-day period. This tabulation included 175 data points, 5 duct speeds, 2 different hot wires (one was broken during the

time period), and many different manipulators. The repeatability of the data was evaluated statistically (i.e., the mean and standard deviation σ) for each of the five duct speeds. At a duct speed of 18.3 m/sec (60.0 ft/sec), the scatter for 95 percent of the data (2σ) fell within ±12 percent of the mean; at 15.24 m/sec (50.0 ft/sec), ±5.7 percent; at 12.2 m/sec (40.4 ft/sec), ±4.5 percent; at 9.1 m/sec (30.0 ft/sec), ±5.7 percent; and at 7.62 m/sec (25.0 ft/sec), ±5.4 percent. Since the 18.3 m/sec (60.0 ft/sec) duct speed was quite noisy and had a relatively large scatter; it was disregarded in most of the data presented herein. The variation in the mean value of measured turbulence $\sigma_{\bar{x}}$ varies inversely as the square root of the number of data points averaged (i.e., $\sigma_{\bar{x}} = \sigma_x/\sqrt{n}$). In other words, the larger the number of values averaged the more accurate the averaged number (mean value). By averaging the turbulence measurements for four speeds (15.24, 12.2, 9.1, and 7.62 m/sec (50.0, 40.0, 30.0, and 25.0 ft/sec)), the error in the mean value decreases by one-half. Assuming that the previously estimated errors for one hot wire apply to each of the other wires in the system, and averaging the turbulence measurements for one manipulator over the four speeds results in an estimated accuracy of 2.5 to 3 percent. Of course, averaging the measured turbulence levels for different mean duct speeds results in a pseudo-turbulence level. However, this pseudo-turbulence level will have less scatter (more accurate) and can be used for relative comparisons of different manipulator configurations.

During the test program, difficulties were sometimes encountered in over driving the amplifiers for the hot-wire instrumentation. This difficulty was resolved by two techniques. The first was to use the dc offset available within the hot-wire signal conditioning equipment. The second was to take two rms-output voltmeter readings: one reading was taken at the desired gain setting (determined by the tape recorder requirements) and the other at the next lower gain setting. The latter two output levels were compared (for acceptance), manually recorded, and averaged in the data reduction process. In general, two additional data points were averaged at each duct speed. This averaging decreased the scatter (or error) in the reported turbulence further.

On the basis of the preceding discussion, it is concluded that the measured and average axial turbulence (pseudo turbulence) data presented is accurate to approximately 2 percent. From the previous discussion (fig. 8), it is estimated that the average lateral turbulence (pseudo turbulence) may have an error as high as 4 percent.

MANIPULATOR CONFIGURATION RESULTS

The results in this section of the paper are presented to answer specific questions which are of a general nature and interest. Some of the items are unusual (i.e., indentation in honeycomb or screens) but could be very significant. The data are presented in tabular form and, when appropriate, also in graphical form. The tabular data presents the measured axial u' and lateral v' turbulence and the averaged pseudo turbulence and a value representing a measure of the total fluctuating velocity component. The latter value is obtained by assuming that the measured lateral and vertical turbulence are equal and then combining all three components $\left(\text{i.e., } \sqrt{[(u')^2 + 2(v')^2]/3}\right)$. The validity of

this approach can be estimated by seeing if $u' = v'$ in the tables. This will provide some insight as to how isotropic the turbulence really is. The tabulated data also include the averaged turbulence over the speed range. This average value may not represent a real condition; however, it will have less error and can be compared relative to that of other configurations.

Logically, it would seem that there should be some relation between the upstream scale of turbulence and the screen mesh size. In other words, a particular mesh screen will result in the greatest turbulence reduction when the screen mesh size is properly matched to the scale of turbulence (size of the disturbance). The integral scale of turbulence is defined as the area under the autocorrelation curve (from time zero to the zero crossing point of the axial component of turbulence) multiplied by the mean velocity. The relationship between the integral scale and the mesh size was looked for but was not found. However, this should not be considered a general conclusion, because the incoming turbulence to each of the manipulators was held constant during this study and because the study was designed specifically for the configuration of the Langley 8-Foot Transonic Pressure Tunnel.

Open Duct Turbulence

Presented in table IV are data for the turbulence measured without any manipulators present. These data are presented for reference only. The data are for the same axial location used when there were manipulators present. This location is approximately 3.69 m (12.11 ft) downstream of the trailing edge of the 45° vanes, measured on the centerline of the duct. This hot-wire location was fixed with respect to the last downstream manipulator. Viscous decay of turbulence has occurred since the fluid has left the cooler. Since the axial and lateral turbulence are not quite equal, the turbulence at the hot-wire location is not quite isotropic.

Reversing Two Different Mesh Screens

The mechanisms involved in changing the turbulence of flow through screens are quite complex. Presumably, the incoming turbulence is changed (momentum change) in passing through the screens, the screens shed their own turbulence, and viscosity is acting continuously. The large-scale turbulence upstream is changed by going through the screen to produce small-scale turbulence which will decay more rapidly due to viscosity. The remaining turbulence is the net effect of the screens. It is generally assumed that, in any series of screens, the finest mesh screens should be last (furthest downstream). Two screens with widely varying mesh size were tested to verify this hypothesis, and the results are given in table V. The order of the two screens was reversed and the tests repeated. In the remarks column of table V, the dashed line signifies a screen and the 42M or 20M indicates the screen mesh sizes (i.e., number of wires per inch). The flow direction is indicated by the arrow. Recall that the hot wires were 0.30 m (12 in.) downstream of the last manipulator. For the coarsest screen, this measuring distance is over 250 screen meshes downstream of the screen. The data in reference 10 indicate that almost all of the turbulence decay occurs within 50 to 75 screen meshes downstream of the screen. The

results in table V indicate that the order of the screens does make a difference, although the difference is not large. It appears that there is a slight gain in performance (reduced turbulence) when the finest screen mesh is placed farthest downstream.

Evaluation of Damaged Screens and Honeycomb

During the test program, the continual handling of the manipulators resulted in inadvertent damage; therefore, an opportunity was available to determine the effect of this damage on the turbulence. The damage was done near the center of the flow channel where the hot wires were generally located (i.e., ±2.54 cm (±1.0 in.) on each side of the duct center and 30.5 cm (12.0 in.) downstream from the last manipulator). For this reason, the measured turbulence resulting from the damage is not equivalent to the average turbulence over the entire duct section, but the worst that would be expected. The resulting measured data are shown in table VI. The sketched cell structure shown in the remarks column indicates the honeycomb location, and the underlying number indicates the honeycomb cell size in inches.

A comparison of the results for damaged and undamaged honeycomb indicates an appreciable increase in the lateral turbulence but little increase in axial turbulence. It should be noted, however, that the additional turbulence created by the damaged honeycomb was processed through two screens before being measured by the hot wire, and screens are very effective in reducing axial turbulence. (See ref. 7.) The damage amounted to perhaps 0.16 cm (0.062 in.) of the trailing edge of some of the honeycomb cells being bent over when inadvertently raked with a bolt of about 0.95 cm (0.375 in.) in diameter.

In table VI(b), the damaged screen was the most downstream screen (i.e., the screen closest to the hot wire). The damage was judged to be very local and mild (i.e., what might occur if a pencil moved down the screen and left a 1/32- to 1/16-in. permanent deformation). The comparison of the damaged and undamaged screens indicates a doubling of the turbulence level. When the fluid passes through the screen, it tends to exit normal to the screen surface. Therefore, any permanent deformation in the screen causes the fluid to exit normal to the deflected surface. These tiny deflected jets cause velocity gradients that in turn generate turbulence. Comparing the damaged-screen data with the open-duct data (table IV), it is seen that the local, mild damage eliminated one-half the benefit of all of the six previous screens. These data point out the importance of not damaging the screens, particularly the last screen.

Screens Against Honeycomb

One manipulator-configuration variable investigated was that of placing the first screen directly against the downstream face of the honeycomb, instead of the more conventional position farther downstream. Presumably, the screen just downstream of the honeycomb assumes full turbulent flow of the fluid leaving the honeycomb-screen combination. (See ref. 12.) For the various configurations tested, the overall axial dimensions were constant, and the distance between the last (farthest downstream) manipulator and the hot wire were also constant. The

data may be compared in table VII. These data are also shown in figure 9. The ordinate of figure 9 is the ratio of the measured turbulence with one of the screens in contact with the downstream surface of the honeycomb to the measured turbulence with the same screen not in contact with the honeycomb. Different symbols are used to represent the ratio for axial and lateral turbulence. The data shown in figure 9 represent the average turbulence (pseudo turbulence) over the speed range. (See discussion of accuracy.) Any data in figure 9 that have an ordinate greater than one indicate that having the screen away from the honeycomb is better, and any values less than one indicate that having the screen against the honeycomb is better. The data in figure 9 indicate that, in general, the axial pseudo turbulence is approximately 10 percent higher and the lateral pseudo turbulence is slightly lower with a screen directly in contact with the honeycomb. Recalling the accuracy limitations of the hot-wire data (see section entitled "Hot-Wire Measuring Accuracy"), it is concluded that there is no performance advantage for either position of the screen directly downstream of the honeycomb. Other considerations such as design, construction, or, possibly, space limitations should be the dictating factors.

Honeycomb at 45° to the Flow Stream

The 45° honeycomb had individual cells aligned with the flow stream; however, the front and back faces of the honeycomb assembly were cut to be parallel to the 45° turning vanes. (See fig. 1 or 2.) It has been suggested that there were some advantages to this configuration, because once the honeycomb interacts with the turbulence coming from the 45° turning vanes, there is a relatively long axial distance (or time) for viscous decay to take place, compared to installation with the honeycomb normal to the flow. There is no such space advantage, however, for the part of the honeycomb near the inside surface of the duct turn. In fact, there is a significant disadvantage because of the high cost of fabricating the 45° honeycomb. A model of this configuration was fabricated and tested, and the results are shown in table VIII.

Before discussing the results, some comments about fabrication difficulties are noteworthy. The honeycomb chosen for this configuration had a 0.318-cm (0.125-in.) cell and 0.0064-cm (0.001-in.) material thickness. The sample was carefully cut from a large, solid block of expanded honeycomb. The remaining machine "burrs" on the two 45° faces were sanded and polished. The resulting faces were not finished as well (as sharp) as those of the 90° honeycomb purchased; however, the final product was as good as could be made with the fabrication procedure used.

The data in table VIII are for three comparable manipulators. The configuration with the screen in contact with the downstream edge of the 45° honeycomb would be expected to be worst, as was true, because the exiting fluid is expected to be turned normal to the screen surface, which in turn establishes shear layers which will generate turbulence. This turbulence generation will not take place when the screens are aligned normal to the mean flow. All the data in table VIII are for the hot wires 30.5 cm (12.0 in.) downstream from the last manipulator (i.e., the 42-mesh screen). The data indicate that the best performance (lowest turbulence) is obtained when the honeycomb and screen surfaces are aligned normal to the flow.

Varying Honeycomb Cell Size

As indicated previously for screens, there is probably some optimum match between the scale of turbulence (in this test, that of the half-scale model of the Langley 8-Foot Transonic Pressure Tunnel) and the honeycomb cell size. The honeycomb cell sizes chosen for evaluation are listed in table II. For these tests, each honeycomb size was tested with the same set of screens. Tests were performed with different sets of screens and high-pass filter settings. No attempt was made to match the screen mesh with the honeycomb cell sizes. The resulting turbulence measurements are tabulated in table IX and shown graphically in figure 10. The data in figure 10 are plotted as the average measured turbulence (pseudo turbulence) over the speed range. The ordinate in figure 10 represents the ratio of the measured turbulence with the honeycomb present to the turbulence without the honeycomb. The fact that the ratios shown are less than one indicates that the honeycomb does reduce the turbulence. In fact, the lower the ratio value (ordinate value) the more effective is the honeycomb. The abscissa in figure 10 is graduated in the four honeycomb cell sizes.

A horizontal line in figure 10 would indicate that the same turbulence reduction occurs for all four honeycomb cell sizes. The data indicate that the 1/8 and 1/4 honeycombs may be superior only because there is one high point for the 1/16 honeycomb and one high point for the 3/8 honeycomb. However, the trend is not consistent (i.e., for all screen combinations). For the screen and honeycomb combination tested, it is concluded that none of the honeycomb cell sizes are consistently superior.

Honeycomb Support Structure

There are indications in reference 10 that the optimum ratio of honeycomb cell length to cell diameter should be about 6. The plenum chamber of the full-scale tunnel is 10.97 m (36.0 ft) in diameter. Currently, honeycomb is not made in large enough pieces to put one piece across the entire section. Further, the honeycomb (with the desired dimensions) might have difficulty supporting itself and the air loads without some additional structure. The problem is to build honeycomb support structure that will generate a minimum of additional turbulence. A sketch of two different honeycomb support structures considered for installation in the full-scale tunnel is shown in figure 11. The measured turbulence for these structures is shown in table X, and the graphical turbulence results, averaged over the speed range (pseudo turbulence), are shown in figure 12.

The two configurations sketched in figure 11 are self-explanatory. A third configuration, not shown, was to place a screen against the downstream honeycomb face and use wire hooks, passing through the cells, to fasten the honeycomb to the screen. This configuration has the added advantage of having one extra screen within the same axial space limitations.

The resulting turbulence measurements (table X) were made directly downstream of the support structure. This was done in order to evaluate the worst possible condition, and therefore, the data presented do not represent the average over the entire cross section.

The data in figure 12 are presented in three groups along the abscissa for the three support structures investigated. To the left of each group is the basic configuration; that is, the configuration without structural support. The data to the right of the base data within each group indicate the turbulence with the support. The data show that the first two configurations increase turbulence, whereas the third configuration reduces turbulence, as might be expected.

SUMMARY OF RESULTS

Tests were conducted on various configurations of honeycomb and screen flow manipulators in a half-scale model of the Langley 8-Foot Transonic Pressure Tunnel. Initially, the experiment was plagued with acoustic noise affecting the hot-wire turbulence measurements. Most of these problems are identified and reduced. The following results are offered:

1. A comparison of the levels of turbulence in the full-scale and half-scale models is good, which indicates that the model could be used to make predicted measurements of alterations to the full-scale tunnel.

2. For two different sizes of screen mesh, there is a slight gain in performance (reduced turbulence) when the finest screen mesh is placed farthest downstream.

3. A slight amount of damage to screens or honeycomb can raise the local (downstream of the damage) turbulence level greatly. This is especially true, of course, for the manipulator farthest downstream.

4. For honeycomb with a cell-length-to-cell-size ratio of about six, there was no performance advantage to mounting the screen against the downstream surface of the honeycomb as opposed to mounting it in a more conventional position farther downstream. However, if the honeycomb requires a support structure, use of a downstream screen to support the honeycomb is an excellent approach. This combination provides improved performance over that of the honeycomb or screens alone.

5. Installing honeycomb along the downstream face of the corner turning vanes with the cells parallel to the flow and front and back faces cut at 45° has no performance advantage over installing honeycomb normal to the flow. The first approach has the disadvantage of being very costly to fabricate.

6. Of the four honeycomb cell sizes tested with various combinations of screens, no cell size had consistently better turbulence reduction. Each of the four honeycombs had a cell-length-to-cell-size ratio of about six.

Langley Research Center
National Aeronautics and Space Administration
Hampton, VA 23665
May 21, 1981

APPENDIX

EQUATIONS FOR AXIAL AND LATERAL TURBULENCE

The equations derived in this appendix are used to determine the axial and lateral turbulence from a single wire at 90° to the flow and from two cross wires at some angle to the flow. The equations are standard equations (e.g., see ref. 13) for using hot wires in a constant temperature mode and are presented herein for completeness:

$$E = f(m,\theta)$$

where

E	output voltage
m	fluid mass-flow rate
θ	angle of flow with respect to the hot-wire probe

The differential of E can be written as

$$dE = \frac{\partial E}{\partial m}\,dm + \frac{\partial E}{\partial \theta}\,d\theta$$

For the low air speeds used herein ($U < 30.0$ m/sec (100.0 ft/sec)), it is permissible to assume that the density is constant so that

$$dE = \frac{\partial E}{\partial U}\,dU + \frac{\partial E}{\partial \theta}\,d\theta$$

and hence

$$\frac{dE}{E} = \frac{\frac{1}{E}\frac{\partial E}{\partial U}}{\frac{1}{U}\frac{\partial U}{\partial U}}\,\frac{dU}{U} + \frac{\frac{1}{E}\frac{\partial E}{\partial \theta}}{}\,d\theta$$

APPENDIX

Let $e = dE$ and $u = dU$ so that

$$\frac{e}{E} = \frac{\partial \ln E}{\partial \ln U}\frac{u}{U} + \frac{\partial \ln E}{\partial \theta}\, d\theta$$

Assume that u and v are small perturbations about the mean

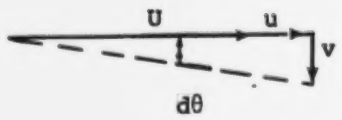

If the flow angle is $d\theta = \arctan \frac{v}{U + u} \approx \frac{v}{U}$, then

$$\frac{e}{E} = \frac{\partial \ln E}{\partial \ln U}\frac{u}{U} + \frac{\partial \ln E}{\partial\, \partial \theta}\frac{v}{U}$$

Let $e' = \frac{e}{E}$, $u' = \frac{u}{U}$, and $v' = \frac{v}{U}$, and multiply by 100 so that e', u', and v' represent percent:

$$e' = \frac{\partial \ln E}{\partial \ln U}\, u' + \frac{\partial \ln E}{\partial \theta}\, v'$$

Define the hot-wire sensitivities by S_1 and S_2, where

$$S_1 = \frac{\partial \ln E}{\partial \ln U}$$

$$S_2 = \frac{\partial \ln E}{\partial \theta}$$

APPENDIX

These sensitivities will be determined by calibration of each individual hot wire. The data reduction equation then becomes

$$e' = S_1 u' + S_2 v'$$

Assume a three-wire system where the axis of one wire is at 90° to the flow and the other two wires are at about ±45° to the flow. The first wire will not respond to v ($S_2 \approx 0$), and therefore,

$$e_1' = S_1 u'$$

For wires 2 and 3:

$$e_2' = S_{12} u' + S_{22} v'$$

$$e_3' = S_{13} u' + S_{23} v'$$

Solve the single-wire equation for the u' component of turbulence,

$$u' = \frac{e_1'}{S_1} \tag{1}$$

Square the two equations for the cross wires, multiply the first by $S_{13}S_{23}$ and the second by $S_{12}S_{22}$, and subtract the two equations so that the cross product term is eliminated and

$$S_{13}S_{23}\left(e_2'^2 - S_{12}^2 u'^2\right) - S_{12}S_{22}\left(e_3'^2 - S_{13}^2 u'^2\right) = \left(S_{13}S_{23}S_{22}^2 - S_{12}S_{22}S_{23}^2\right) v'^2$$

Solve for v' and recall that the u' component of turbulence is known from the single wire (eq. (1)) so that:

$$v'^2 = \frac{S_{13}S_{23}\left(e_2'^2 S_{12}^2 u'^2\right) - S_{12}S_{22}\left(e_3'^2 - S_{13}^2 u'^2\right)}{S_{13}S_{23}S_{22}^2 - S_{12}S_{22}S_{23}^2} \tag{2}$$

This is the lateral component of turbulence.

APPENDIX

The sensitivity of the single wire S_1 is determined by measuring the wire output (dc volts) over the speed range U of interest and determining the slope for a plot of $\ln E$ versus $\ln U \left(S_1 = \frac{\partial \ln E}{\partial \ln U} \right)$. Similarly, the sensitivities S_{21} and S_{31} are determined for the other two cross wires. The sensitivities S_{22} and S_{32} are determined by measuring the cross-wire dc-voltage output for a number of small angle variations θ. The sensitivities are then determined from the slope of a plot of $\ln E$ versus $\theta \left(S_2 = \frac{\partial \ln E}{\partial \theta} \right)$ for the two cross wires. These sensitivities must be measured in a relatively low-turbulence environment. Since these sensitivities (S_{22}, S_{32}) vary somewhat with speed, they are determined for various speeds and they are expanded and redefined as follows:

$$\left.\begin{aligned} S_{22} &= L_{21}U + L_{22} \\ S_{32} &= L_{31}U + L_{32} \end{aligned}\right\} \qquad (3)$$

REFERENCES

1. Braslow, Albert L.; and Muraca, Ralph J.: A Perspective of Laminar-Flow Control. AIAA Paper 78-1528, Aug. 1978.

2. Dougherty, N. S., Jr.; and Fisher, D. F.: Boundary-Layer Transition on a 10-Deg Cone: Wind Tunnel/Flight Correlation. AIAA-80-0154, Jan. 1980.

3. Keefe, Laurence R.: A Study of Acoustic Fluctuations in the Langley 8-Foot Transonic Pressure Tunnel. NASA CR-158983, 1979.

4. Owen, F. Kevin; Stainback, P. Calvin; and Harvey, William D.: Evaluation of Flow Quality in Two NASA Transonic Wind Tunnels. AIAA Paper 79-1532, July 1979.

5. Brooks, Joseph D.; Stainback, P. Calvin; and Brooks, Cuyler W., Jr.: Additional Flow Quality Measurements in the Langley Research Center 8-Foot Transonic Pressure Tunnel. A Collection of Technical Papers - AIAA 11th Aerodynamic Testing Conference, Mar. 1980, pp. 138-145. (Available as AIAA-80-0434.)

6. McKinney, Marion O.; and Scheiman, James: Evaluation of Turbulence Reduction Devices for the Langley 8-Foot Transonic Pressure Tunnel. NASA TM-81792, 1981.

7. Scheiman, James; and Brooks, J. D.: A Comparison of Experimental and Theoretical Turbulence Reduction From Screens, Honeycomb and Honeycomb-Screen Combinations. A Collection of Technical Papers - AIAA 11th Aerodynamic Testing Conference, Mar. 1980, pp. 129-137. (Available as AIAA-80-0433.)

8. Johnson, William G., Jr.; and Igoe, William B.: Aerodynamic Characteristics at Low Reynolds Numbers of Several Heat-Exchanger Configurations for Wind-Tunnel Use. NASA TM-80188, 1979.

9. Schubauer, G. B.; Spangenberg, W. G.; and Klebanoff, P. S.: Aerodynamic Characteristics of Damping Screens. NACA TN 2001, 1950.

10. Loehrke, R. I.; and Nagib, H. M.: Experiments on Management of Free-Stream Turbulence. AGARD-R-598, Sept. 1972.

11. Kershner, David D.: Miniature Flow-Direction and Airspeed Sensor for Airplanes and Radio-Controlled Models in Spin Studies. NASA TP-1467, 1979.

12. Wigeland, R. A.; Tan-atichat, J.; and Nagib, H M.: Evaluation of a New Concept for Reducing Free-Stream Turbulence in Wind Tunnels. AIAA-80-0432-CP, Mar. 1980.

13. Hinze, J. O.: Turbulence. McGraw-Hill Book Co., Inc., 1959.

TABLE I.- FINNED-TUBE COOLER*

Dimension	Full scale		Half scale	
	cm	in.	cm	in.
Tube outside diameter	2.54	1.00	1.27	0.500
Fin outside diameter	5.59	2.20	2.86	1.125
Fin spacing	8 fins/2.54 cm	8 fins/in.	14 fins/2.54 cm	14 fins/in.
Lateral spacing	8.08	3.18	5.08	2.00
Axial spacing	4.65	1.83	2.26	.89

*Fin thickness not scaled.

TABLE II.- PHYSICAL PROPERTIES OF MANIPULATOR

Screens

Symbol	Mesh (wires/2.54 cm)	Wire diam., mm (in.)	Open area, percent
4M	4	1.27 (0.050)	64
8M	8	.660 (.026)	63
20M	20	.229 (.009)	67
28M	28	.190 (.0075)	62
36M	36	.165 (.0065)	59
42M	42	.140 (.0055)	59

Honeycomb

Symbol	Cell size, cm (in.)	Cell length, cm (in.)	Material thickness, mm (in.)
1/16 HC	0.159 (1/16)	1.27 (0.50)	0.0254 (0.001)
1/8 HC	.318 (1/8)	1.90 (.75)	.0254 (.001)
1/4 HC'	.635 (1/4)	3.81 (1.50)	.0254 (.001)
1/4 HC	.635 (1/4)	3.81 (1.50)	.0762 (.003)
3/8 HC	.952 (3/8)	7.62 (3.00)	.0762 (.003)

TABLE III.- ACOUSTICS OF HALF-SCALE MODEL

(a) Noise from cooler

Duct velocity		Measured acoustic frequency,[a] Hz				Computed Strouhal frequency,[b] Hz	
		Microphone No. 1		Microphone No. 2			
m/sec	ft/sec	1st harmonic	2nd harmonic	1st harmonic	2nd harmonic	1st harmonic	2nd harmonic
7.62	25	195	315	192	315	186	372
9.10	30	225	357	228	---	223	446
12.20	40	300	590	300	580	298	596
15.24	50	380	730	375	720	372	744

[a]Both microphones out of duct.

[b] $f = \frac{S_t U}{d}$ where $S_t = 0.31$, U = Duct speed, and d = 1.27 cm (0.5 in.).

(b) Standing waves within duct

Duct velocity		Measured turbulence frequency, Hz									Measured acoustic frequency, Hz (microphone No. 2 in duct)				
		Hot wire No. 2 (single wire)					Hot wire No. 4 (single wire)								
m/sec	ft/sec														
7.62	25	14	--	35	45	59	14	35	45	59	8	24	44	57	90
9.10	30	14	20	36	--	56	13	35	55	--	10	25	48	58	90
12.20	40	14	--	34	--	59	14	--	--	--	9	24	47	58	98
15.24	50	--	--	--	--	--	--	--	--	--	8	24	46	58	90

Computed standing-wave frequency, Hz, for wavelength -				
1/4 ℓ	3/4 ℓ	5/4 ℓ	7/4 ℓ	11/4 ℓ
8.0	24.0	40	56	88

TABLE IV.- TURBULENCE OF OPEN DUCT (NO MANIPULATORS)

Run no.	U_{ref}, m/sec (ft/sec)	u'	v'	$\sqrt{\frac{(u')^2 + 2(v')^2}{3}}$
711	14.9 (48.9)	1.58	1.82	1.74
712	12.0 (39.3)	1.44	1.72	1.64
713	8.9 (29.3)	1.26	1.48	1.41
714	7.4 (24.4)	1.12	1.34	1.27
Av		1.35	1.59	1.52
828	15.2 (50.0)	1.58	1.70	1.66
829	12.0 (39.5)	1.42	1.57	1.52
830	9.0 (29.6)	1.24	1.44	1.38
831	7.6 (24.8)	1.12	1.30	1.25
Av		1.34	1.50	1.45

TABLE V.- TURBULENCE WHEN REVERSING ORDER OF TWO DIFFERENT MESH SCREENS

Run no.	U_{ref}, m/sec (ft/sec)	u'	v'	$\sqrt{\frac{(u')^2 + 2(v')^2}{3}}$	Remarks
481	14.9 (48.8)	1.00	1.30	1.20	
482	12.2 (40.0)	.96	1.30	1.20	
483	9.0 (29.4)	.96	1.35	1.23	
484	7.6 (25.0)	.90	1.38	1.24	
Av		.95	1.33	1.22	42M 20M High pass, 100 Hz
485	15.0 (49.2)	1.03	1.45	1.32	
486	12.3 (40.3)	1.02	1.23	1.16	
487	9.9 (32.6)	.96	1.43	1.30	
488	7.7 (25.3)	.92	1.48	1.32	
Av		.98	1.40	1.28	20M 42M High pass, 100 Hz

TABLE VI.- EVALUATION OF TURBULENCE DUE TO DAMAGED SCREEN AND DAMAGED HONEYCOMB

(a) Damaged and undamaged honeycomb

Run no.	U_{ref}, m/sec (ft/sec)	u'	v'	$\sqrt{\frac{(u')^2 + 2(v')^2}{3}}$	Remarks
363	15.6 (51.1)	0.56	1.67	1.40	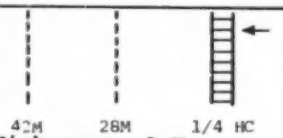 High-pass, 2-Hz, damaged honeycomb
364	12.4 (40.8)	.50	1.51	1.27	
365	9.3 (30.5)	.45	1.35	1.13	
366	7.7 (25.4)	.44	1.32	1.11	
Av		.49	1.46		
367	15.6 (51.3)	0.49	0.36	0.41	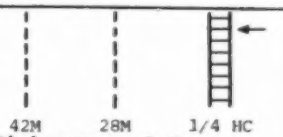 High-pass, 2-Hz, undamaged honeycomb
368	12.5 (40.9)	.47	.40	.42	
369	9.3 (30.6)	.41	.39	.40	
370	7.8 (25.5)	.36	.38	.37	
Av		.43	.38		

(b) Damaged and undamaged last screen

Run no.	U_{ref}, m/sec (ft/sec)	u'	v'	$\sqrt{\frac{(u')^2 + 2(v')^2}{3}}$	Remarks
783	15.3 (50.2)	0.97	0.82	0.87	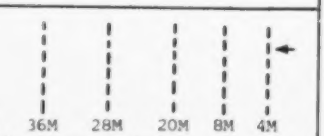 High-pass, 100-Hz, damaged last screen
784	11.9 (39.2)	.97	.88	.91	
785	9.1 (29.8)	.94	.93	.93	
786	7.6 (24.8)	.84	.90	.88	
Av		.93	.88		
787	15.0 (49.3)	0.38	0.43	0.42	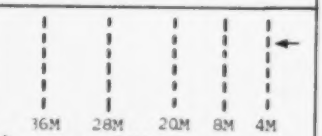 High-pass, 100-Hz, undamaged screen
788	11.9 (39.0)	.39	.44	.43	
789	8.9 (29.3)	.33	.50	.45	
790	7.5 (24.5)	.18	.25	.23	
Av		.32	.41		

TABLE VII.- COMPARISON OF TURBULENCE FOR HONEYCOMB AND SCREENS WHEN ONE SCREEN IS AGAINST HONEYCOMB AND WHEN SCREEN IS NOT AGAINST HONEYCOMB (FIG. 9)

(a) Configuration A

Run no.	U_{ref}, m/sec (ft/sec)	u'	v'	$\sqrt{\frac{(u')^2 + 2(v')^2}{3}}$	Remarks
291	15.5 (51.0)	0.41	0.28	0.33	
292	12.4 (40.6)	.40	.29	.33	
293	9.3 (30.4)	.38	.21	.28	
294	7.7 (25.3)	.25	.16	.19	
295	6.2 (20.2)	.26	.12	.18	
Av		.34	.21	.26	High pass, 2 Hz
296	15.7 (51.4)	0.44	0.24	0.32	
297	12.5 (41.0)	.46	.21	.32	
298	9.3 (30.6)	.38	.12	.24	
299	7.8 (25.5)	.26	.03	.15	
300	6.2 (20.4)	.29	.05	.17	
Av		.37	.13	.24	High pass, 2 Hz

TABLE VII.- Continued

(b) Configuration B

Run no.	U_{ref}, m/sec (ft/sec)	u'	v'	$\sqrt{\frac{(u')^2 + 2(v')^2}{3}}$	Remarks
320	15.7 (51.6)	0.45	0.38	0.40	
321	12.6 (41.2)	.43	.39	.40	
322	9.3 (30.6)	.44	.28	.34	
323	7.7 (25.4)	.39	.25	.30	
324	6.2 (20.3)	.43	.13	.27	
Av		.43	.29	.34	High pass, 2 Hz
325	15.6 (51.3)	0.49	0.40	0.43	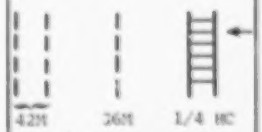
326	12.5 (40.9)	.50	.32	.39	
327	9.3 (30.6)	.45	.32	.37	
328	7.8 (25.5)	.39	.29	.33	
329	6.2 (20.4)	.41	.24	.31	
Av		.45	.31	.37	High pass, 2 Hz

(c) Configuration C

Run no.	U_{ref}, m/sec (ft/sec)	u'	v'	$\sqrt{\frac{(u')^2 + 2(v')^2}{3}}$	Remarks
346	15.5 (51.0)	0.56	0.46	0.50	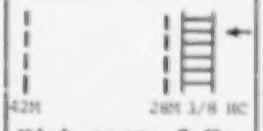
347	12.4 (40.7)	.54	.38	.44	
348	9.3 (30.5)	.47	.31	.37	
349	7.7 (25.4)	.41	.33	.36	
Av		.50	.37	.42	High pass, 2 Hz
351	15.6 (51.1)	0.50	0.44	0.46	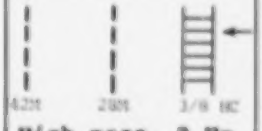
352	12.4 (40.8)	.46	.44	.45	
355	9.3 (30.6)	.41	.39	.40	
356	7.7 (25.4)	.36	.30	.32	
Av		.43	.39	.41	High pass, 2 Hz

TABLE VII.- Concluded

(d) Configuration D

Run no.	U_{ref}, m/sec (ft/sec)	u'	v'	$\sqrt{\frac{(u')^2 + 2(v')^2}{3}}$	Remarks
375	15.6 (51.1)	0.46	0.31	0.37	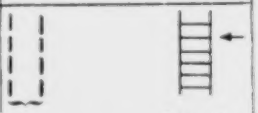
376	12.4 (40.8)	.48	.35	.40	
377	9.3 (30.5)	.42	.40	.41	
378	7.7 (25.4)	.35	.42	.40	
Av		.43	.37	.40	High pass, 2 Hz
380	15.5 (50.9)	0.52	0.52	0.52	
381	12.4 (40.6)	.48	.53	.51	
382	9.3 (30.4)	.47	.28	.35	
383	7.7 (25.3)	.38	.17	.26	
Av		.46	.38	.41	High pass, 2 Hz

(e) Configuration E

Run no.	U_{ref}, m/sec (ft/sec)	u'	v'	$\sqrt{\frac{(u')^2 + 2(v')^2}{3}}$	Remarks
746	15.0 (49.4)	0.59	0.52	0.55	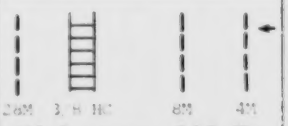
747	12.0 (39.4)	.54	.52	.52	
748	9.0 (29.6)	.55	.50	.52	
749	7.6 (24.9)	.56	.41	.46	
Av		.56	.49	.51	High pass, 100 Hz
750	15.1 (49.6)	0.69	0.52	0.58	
751	12.0 (39.4)	.67	.46	.54	
752	9.0 (29.5)	.66	.45	.53	
753	7.5 (24.7)	.63	.38	.48	
Av		.66	.45	.53	High pass, 100 Hz

TABLE VIII.- COMPARISON OF TURBULENCE REDUCTION FOR HONEYCOMB AT 45° AND 90° TO MEAN FLOW

Run no.	U_{ref}, m/sec (ft/sec)	u'	v'	$\sqrt{\frac{(u')^2 + 2(v')^2}{3}}$	Remarks
251	21.8 (71.5)	1.34	0.95	1.10	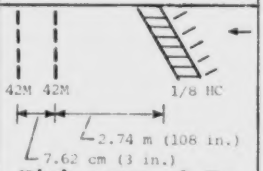
252	18.6 (61.0)	1.25	1.06	1.13	
253	15.4 (50.7)	1.13	1.02	1.06	
254	12.3 (40.5)	1.05	.88	.94	
255	9.2 (30.3)	1.03	.67	.81	
Av		1.16	.92		High pass, 2 Hz
262	21.8 (71.6)	1.41	1.19	1.27	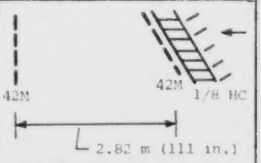
263	18.6 (61.2)	1.27	1.20	1.22	
264	15.5 (50.8)	1.16	1.07	1.10	
265	12.4 (40.6)	1.12	.95	1.01	
266	9.3 (30.4)	1.06	.83	.91	
Av		1.20	1.05		High pass, 2 Hz
225	21.6 (70.9)	1.14	0.27	0.69	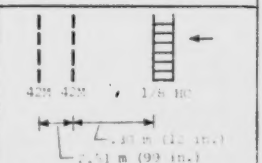
226	18.5 (60.6)	1.08	.52	.75	
227	15.4 (50.4)	1.00	.31	.63	
228	12.2 (40.2)	.90	.36	.60	
230	9.2 (30.1)	.79	.38	.55	
Av		.98	.37		High pass, 2 Hz

TABLE IX.- MEASURED TURBULENCE FOR VARIOUS HONEYCOMB CELL SIZES WHEN OPERATING WITH DIFFERENT SCREEN COMBINATIONS (FIG. 10)

(a) Screen configuration A

Run no.	U_{ref}, m/sec (ft/sec)	u'	v'	$\sqrt{\frac{(u')^2 + 2(v')^2}{3}}$	Remarks
465	15.4 (50.5)	0.51	0.72	0.66	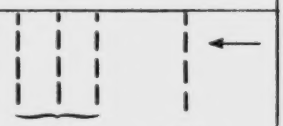
466	12.3 (40.3)	.49	.70	.64	
467	9.2 (30.2)	.46	.63	58	
468	7.6 (25.1)	.45	.65	.59	
Av		.48	.68	.62	High-pass, 2-Hz, without honeycomb
489	15.2 (50.0)	0.53	0.30	0.40	
490	12.6 (41.5)	.48	.21	.32	
491	9.4 (30.7)	.46	.15	.29	
492	7.6 (25.0)	.35	.15	.23	
Av		.45	.20	.31	High pass, 2 Hz
493	15.1 (49.7)	0.51	0.20	0.33	
494	12.2 (39.9)	.49	.20	.33	
495	9.0 (29.6)	.48	.13	.30	
496	7.6 (24.8)	.36	.14	.23	
Av		.46	.17	.30	High pass, 2 Hz
498	15.2 (49.8)	0.54	0.19	0.35	
499	12.5 (41.0)	.48	.20	.32	
500	10.0 (32.7)	.46	.21	.31	
501	7.6 (24.8)	.34	.10	.21	
Av		.45	.18	.30	High pass, 2 Hz
502	15.1 (49.7)	0.48	0.19	0.32	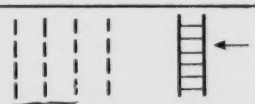
503	12.3 (40.4)	.45	.20	.30	
504	9.3 (30.4)	.44	.15	.28	
505	7.4 (24.2)	.32	.14	.22	
Av		.42	.17	.28	High pass, 2 Hz

TABLE IX.- Continued

(b) Screen configuration B

Run no.	U_{ref}, m/sec (ft/sec)	u'	v'	$\sqrt{\frac{(u')^2 + 2(v')^2}{3}}$	Remarks
584	15.2 (49.8)	0.81	0.80	0.80	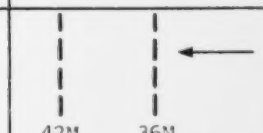
585	12.4 (40.8)	.76	.73	.74	
586	9.3 (30.4)	.72	.66	.68	
587	7.7 (25.2)	.64	.68	.67	
Av		.73	.72	.72	High pass, 100 Hz
568	15.3 (50.1)	0.60	0.27	0.42	
569	12.4 (40.7)	.56	.17	.35	
570	9.9 (32.6)	.59	.34	.44	
571	7.8 (25.6)	.50	.46	.47	
Av		.56	.31	.42	High pass, 100 Hz
572	15.4 (50.7)	0.45	0.33	0.37	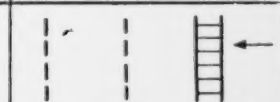
573	12.4 (40.7)	.38	.39	.39	
574	9.5 (31.3)	.42	.33	.36	
575	7.6 (24.8)	.28	.24	.26	
Av		.38	.32	.34	High pass, 100 Hz
576	15.7 (51.4)	0.48	0.32	0.38	
577	12.8 (41.9)	.49	.28	.36	
578	9.7 (31.7)	.46	.35	.39	
579	7.9 (25.8)	.37	.32	.34	
Av		.45	.32	.37	High pass, 100 Hz
580	15.4 (50.4)	0.46	0.48	0.48	
581	12.7 (41.6)	.46	.50	.49	
582	9.7 (31.9)	.44	.51	.49	
583	7.7 (25.4)	.37	.53	.48	
Av		.43	.51	.48	High pass, 100 Hz

TABLE IX.- Concluded

(c) Screen configuration C

Run no.	U_{ref}, m/sec (ft/sec)	u'	v'	$\sqrt{\frac{(u')^2 + 2(v')^2}{3}}$	Remarks
135	21.8 (71.6)	1.28	1.41	1.37	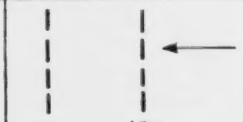
136	18.6 (61.2)	1.26	1.35	1.32	
137	15.5 (50.9)	1.09	1.40	1.30	
138	12.4 (40.6)	1.04	1.35	1.26	
139	9.3 (30.4)	.91	1.36	1.23	
Av		1.12	1.37		High pass, 2 Hz
219	21.6 (70.9)	1.22	0.56	0.84	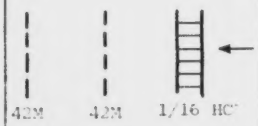
220	18.4 (60.5)	1.06	.64	.80	
221	15.3 (50.3)	.99	.49	.70	
222	12.2 (40.2)	.92	.47	.66	
224	9.2 (30.1)	.87	.28	.55	
Av		1.01	.49		High pass, 2 Hz
225	21.6 (70.9)	1.14	0.27	0.69	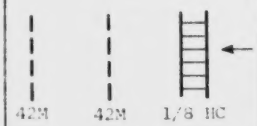
226	18.5 (60.6)	1.08	.52	.75	
227	15.4 (50.4)	1.00	.31	.63	
228	12.2 (40.2)	.90	.36	.60	
230	9.2 (30.1)	.79	.38	.55	
Av		.98	.37		High pass, 2 Hz
232	21.6 (71.0)	1.14	0.54	0.76	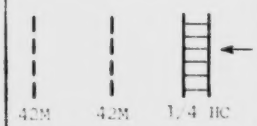
233	18.5 (60.7)	1.08	.94	.99	
234	15.4 (50.5)	1.00	.40	.66	
235	12.3 (40.3)	.95	.34	.61	
236	9.2 (30.2)	.78	.43	.57	
Av		.99	.53		High pass, 2 Hz
246	21.6 (70.9)	1.21	0.77	0.94	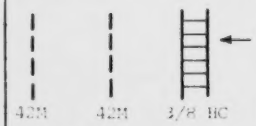
247	18.4 (60.5)	1.10	.60	.80	
248	15.3 (50.3)	.97	.54	.71	
249	12.2 (40.2)	.91	.50	.67	
250	9.2 (30.1)	.78	.52	.62	
Av		.99	.59		High pass, 2 Hz

TABLE X.- COMPARISON OF TURBULENCE WITH VARIOUS HONEYCOMB SUPPORT STRUCTURES (FIG. 12)

Run no.	U_{ref}, m/sec (ft/sec)	u'	v'	$\sqrt{\frac{(u')^2 + 2(v')^2}{3}}$	Remarks
(a) Configuration A without honeycomb support					
498	15.2 (49.8)	0.54	0.19	0.35	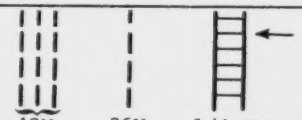
499	12.5 (41.0)	.48	.20	.32	
500	10.0 (32.7)	.46	.21	.31	
501	7.6 (24.8)	.34	.10	.21	
Av		.45	.18	.30	42M 36M 1/4 HC High pass, 2 Hz
(b) Configuration A with honeycomb support (fig. 11(a))					
506	14.6 (48.0)	0.56	0.44	0.48	
507	12.1 (39.6)	.52	.41	.45	
508	9.3 (30.4)	.53	.40	.45	
509	7.6 (25.0)	.43	.38	.40	
Av		.51	.40	.44	1/4 HC 42M 36M Vane support High pass, 2 Hz; both hot wires 2.54 cm off ℄
510	14.9 (48.9)	0.55	0.26	0.38	
511	12.1 (39.6)	.53	.27	.38	
512	9.7 (31.9)	.54	.27	.28	
513	7.5 (24.7)	.45	.23	.32	
Av		.52	.26	.37	1/4 HC 42M 36M Vane support High pass, 2 Hz; cross wire on ℄; single wire 5.08 cm off center
514	14.9 (49.0)	0.50	0.39	0.43	
515	12.1 (39.7)	.47	.40	.42	
516	9.2 (30.1)	.50	.41	.44	
517	7.5 (24.6)	.37	.39	.38	
Av		.46	.39	.42	1/4 HC 42M 36M Vane support High pass, 2 Hz; single wire on ℄; cross wire 5.08 cm off center
(c) Configuration B without honeycomb support					
608	14.9 (48.9)	0.39	0.14	0.25	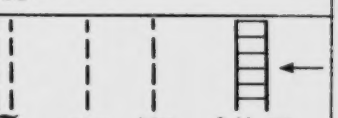
609	12.1 (39.7)	.38	.12	.24	
610	9.0 (29.5)	.30	.09	.19	
611	7.6 (24.9)	.18	.11	.14	
Av		.31	.12		42M 36M 36M 1/4 HC High pass, 100 Hz

TABLE X.- Concluded

Run no.	U_{ref}, m/sec (ft/sec)	u'	v'	$\sqrt{\frac{(u')^2 + 2(v')^2}{3}}$	Remarks
(d) Configuration B with honeycomb support (fig. 11(b))					
612	14.9 (48.8)	0.51	0.23	0.35	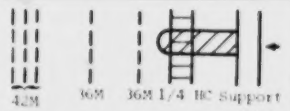
613	12.0 (39.3)	.44	.33	.37	
614	8.9 (29.2)	.37	.30	.33	
615	7.5 (24.5)	.21	.18	.19	
Av		.38	.26		High pass, 100 Hz
(e) Configuration B with honeycomb screen support					
616	15.0 (49.1)	0.48	0.12	0.29	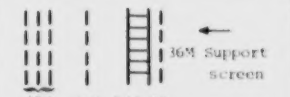
617	11.9 (39.0)	.48	.07	.28	
618	8.9 (29.2)	.44	.20	.30	
619	7.5 (24.7)	.25	.11	.17	
Av		.41	.13		High pass, 100 Hz
(f) Configuration C without honeycomb support					
624	15.2 (49.9)	0.49	0.05	0.29	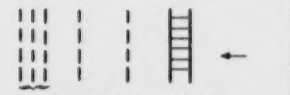
625	12.1 (39.7)	.48	.12	.29	
626	9.0 (29.4)	.50	.36	.41	
627	7.6 (24.9)	.42	.38	.39	
Av		.47	.23	.35	High pass, 100 Hz
(g) Configuration C with honeycomb screen support					
620	15.2 (50.0)	0.48	0.19	0.32	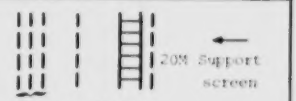
621	12.1 (39.6)	.46	.18	.30	
622	9.0 (29.5)	.38	.08	.23	
623	7.6 (24.9)	.28	.14	.20	
Av		.40	.15		High pass, 100 Hz

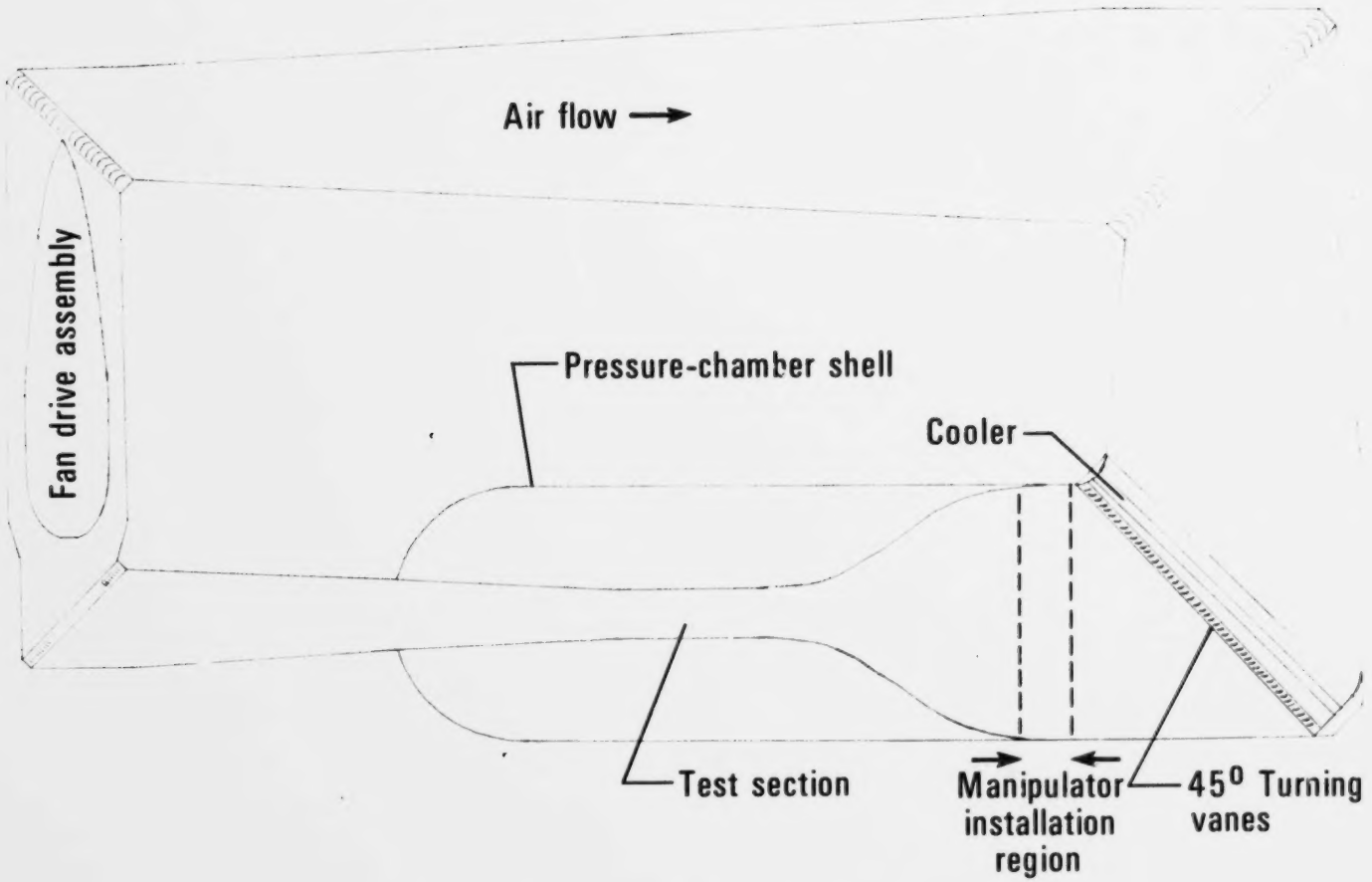

Figure 1.- Sketch of Langley 8-Foot Transonic Pressure Tunnel.

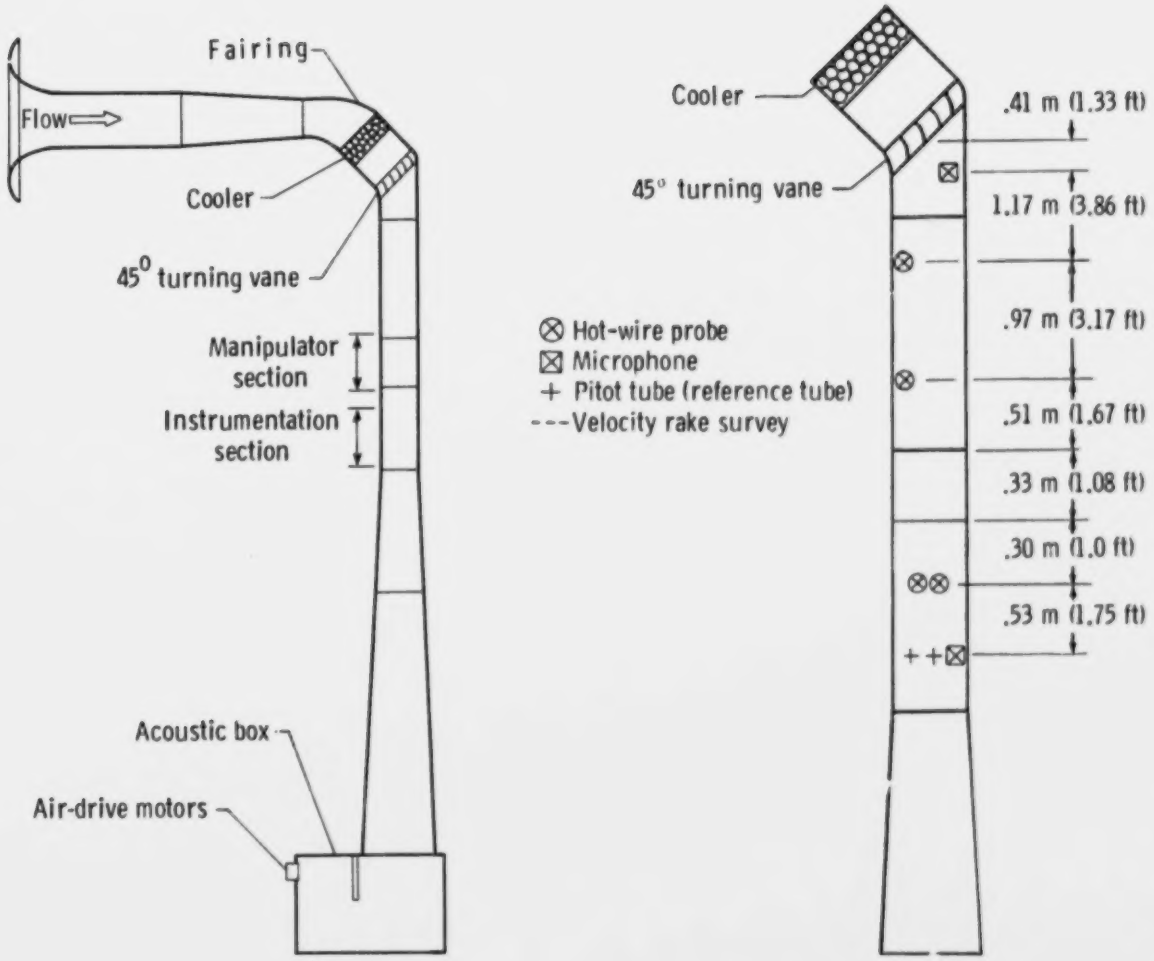

(a) Overall view.

(b) General dimensions.

Figure 2.- Sketch of half-scale model used in turbulence reduction program.

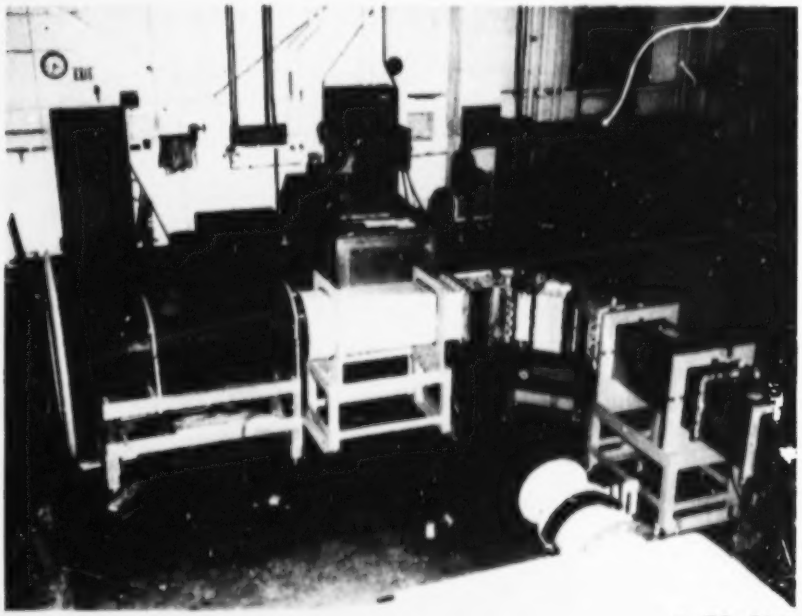

L-79-625

(a) Half-scale model duct.

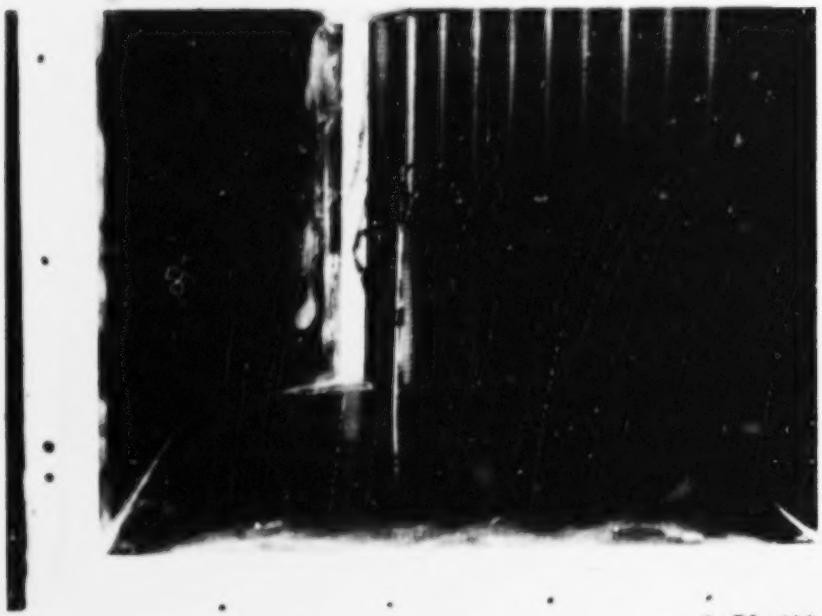

L-79-628

(b) Half-scale cooler.

Figure 3.- Photographs of half-scale test model and cooler.

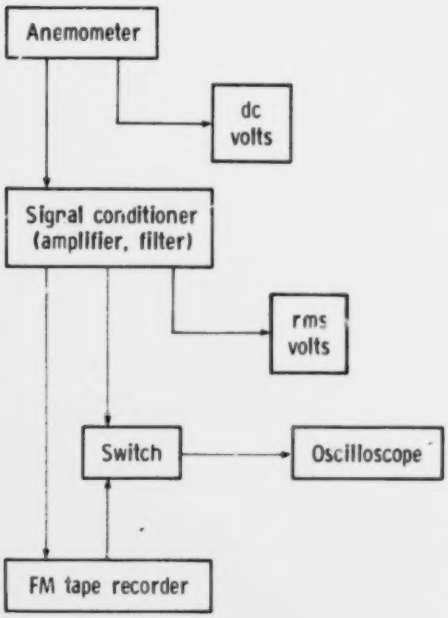

(a) Single-wire sensor.

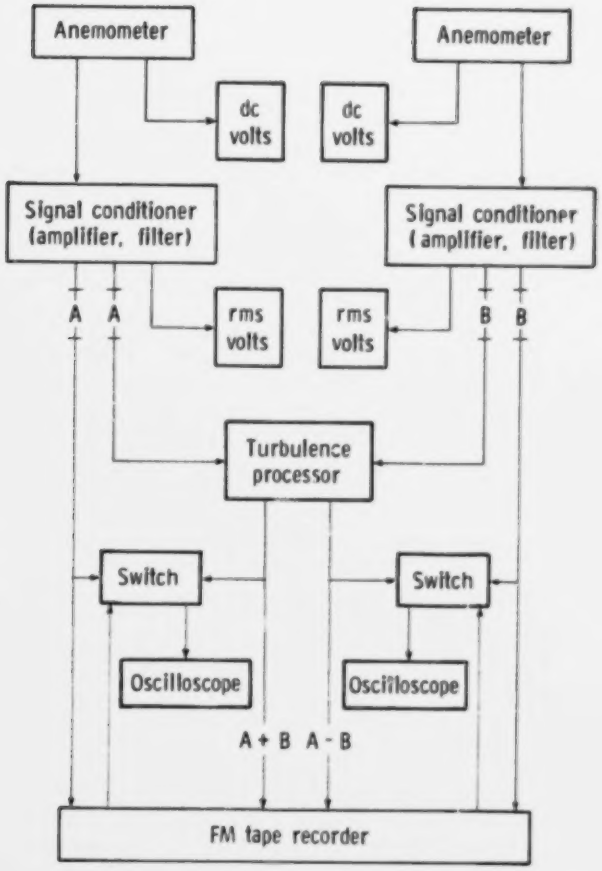

(b) Cross-wire sensors.

Figure 4.- Hot-wire circuit diagram.

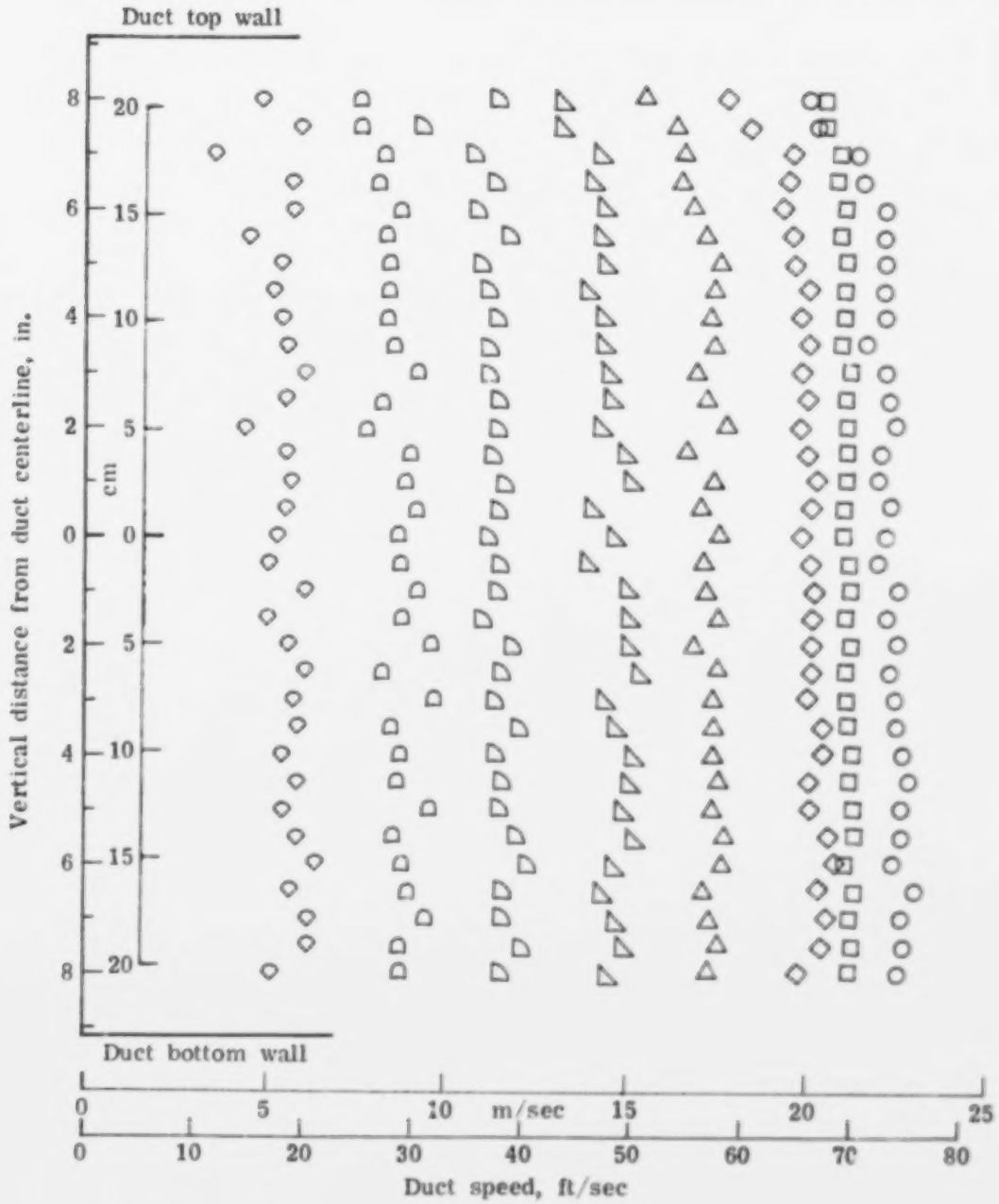

(a) Vertical velocity survey along centerline of duct.

Figure 5.- Vertical and lateral velocity survey through horizontal and vertical centerline of duct. Survey station is 43.2 cm (17 in.) downstream of trailing edge of 45° vanes on duct centerline. Symbols represent various reference speeds.

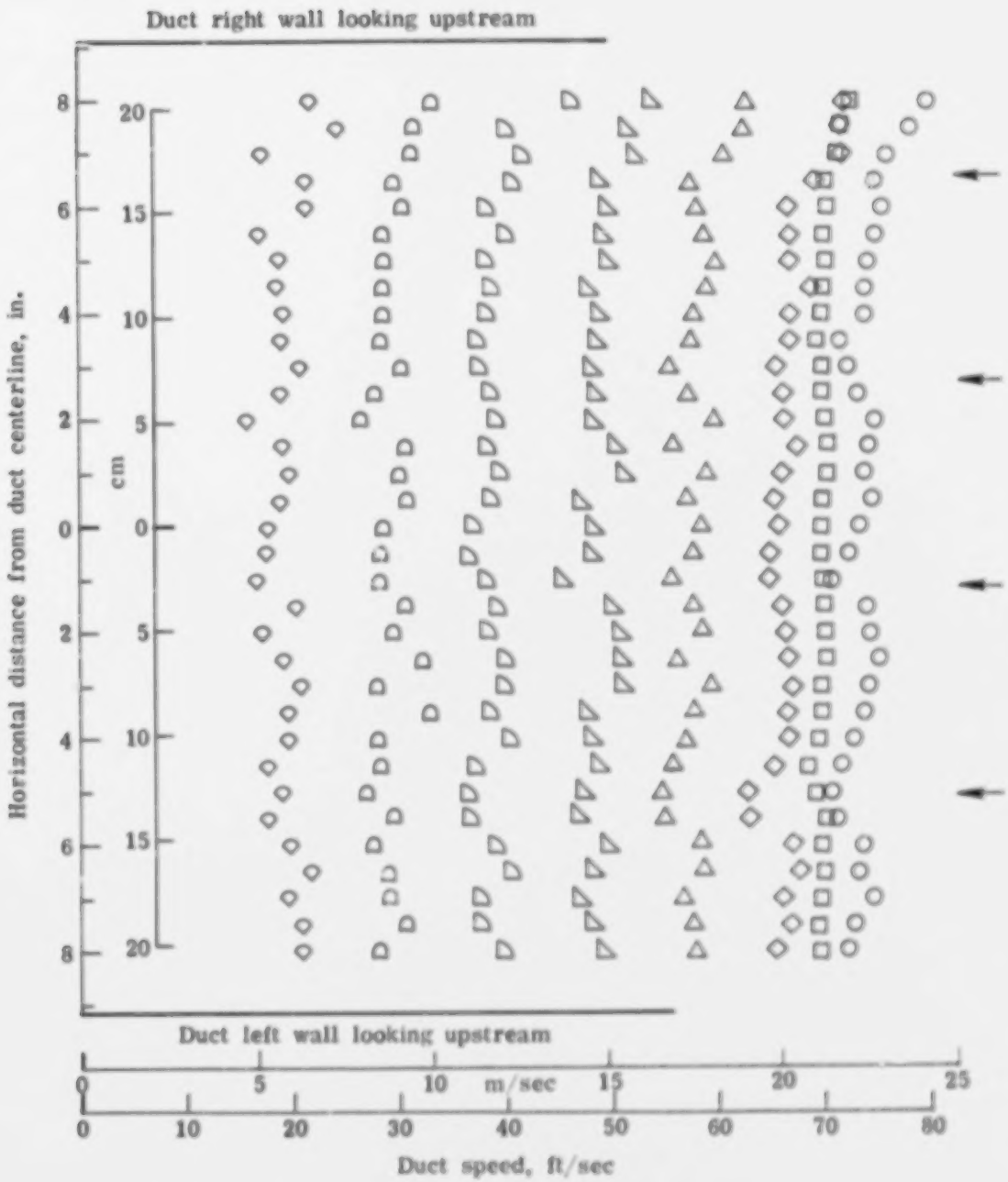

(b) Lateral velocity survey along centerline of duct.

Figure 5.- Concluded.

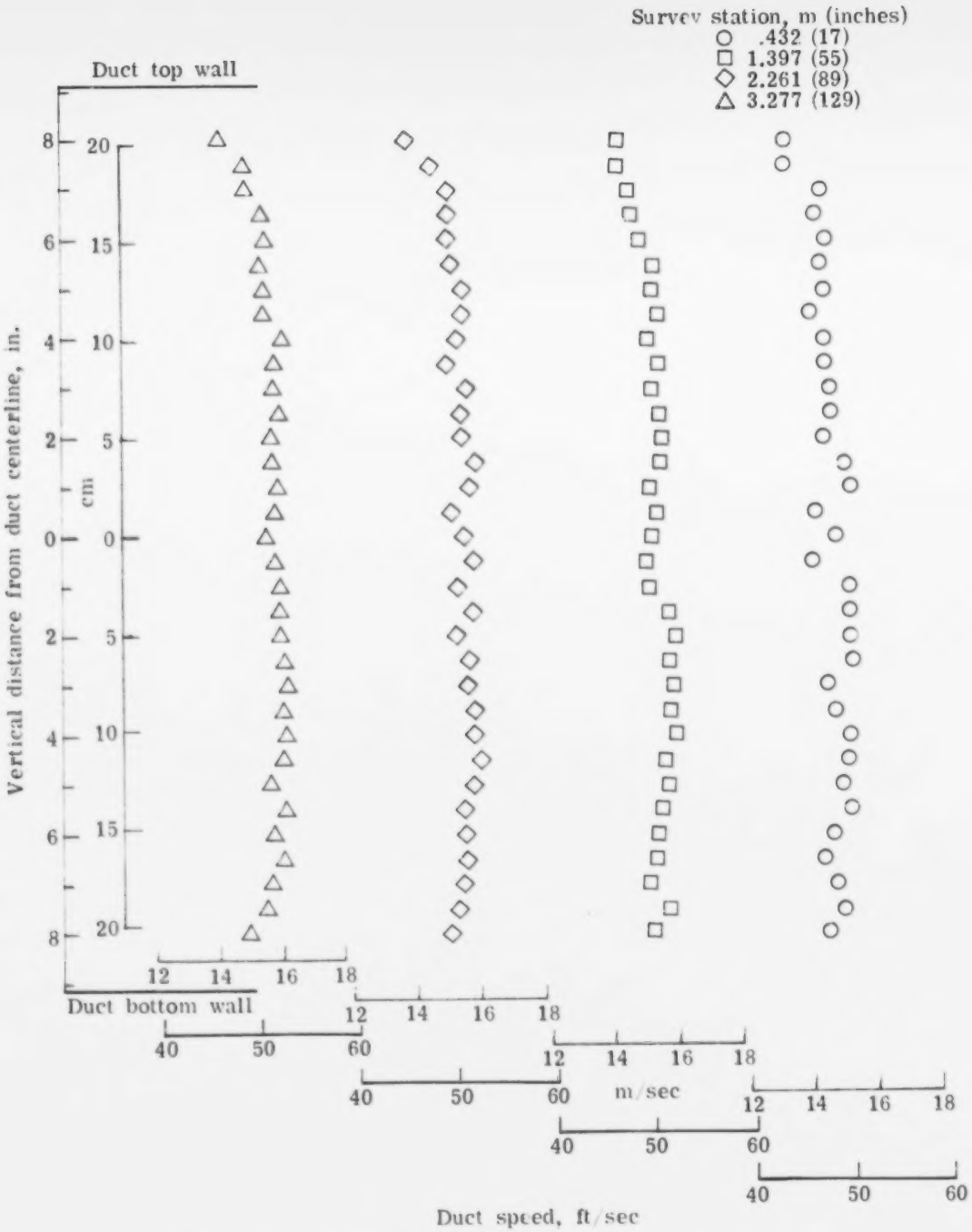

(a) Vertical velocity survey along centerline of duct.

Figure 6.- Vertical and lateral velocity survey through horizontal and vertical centerline of duct. Survey station noted is distance downstream of trailing edge of 45° vanes on duct centerline.

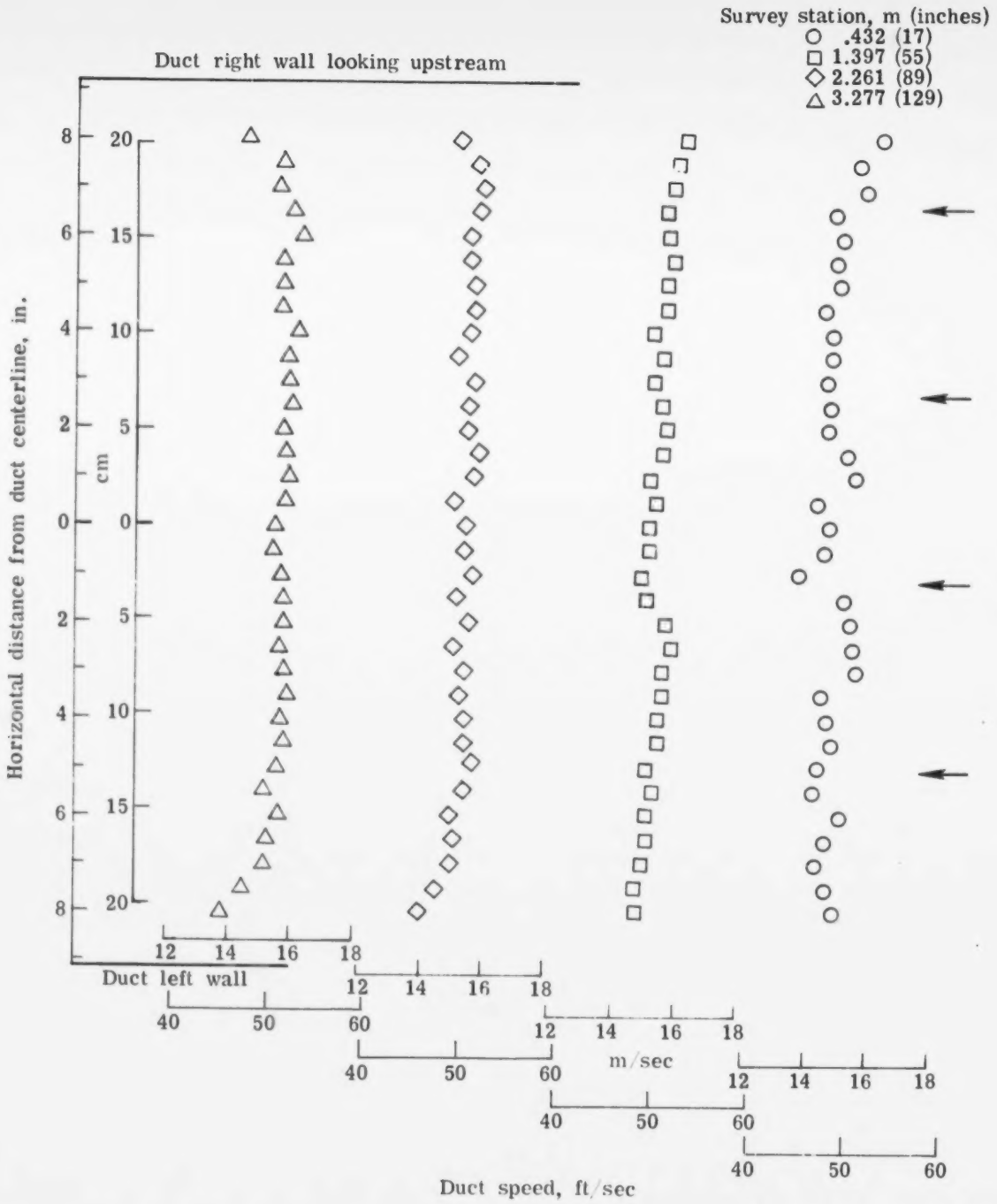

(b) Lateral velocity along centerline of duct.

Figure 6.- Concluded.

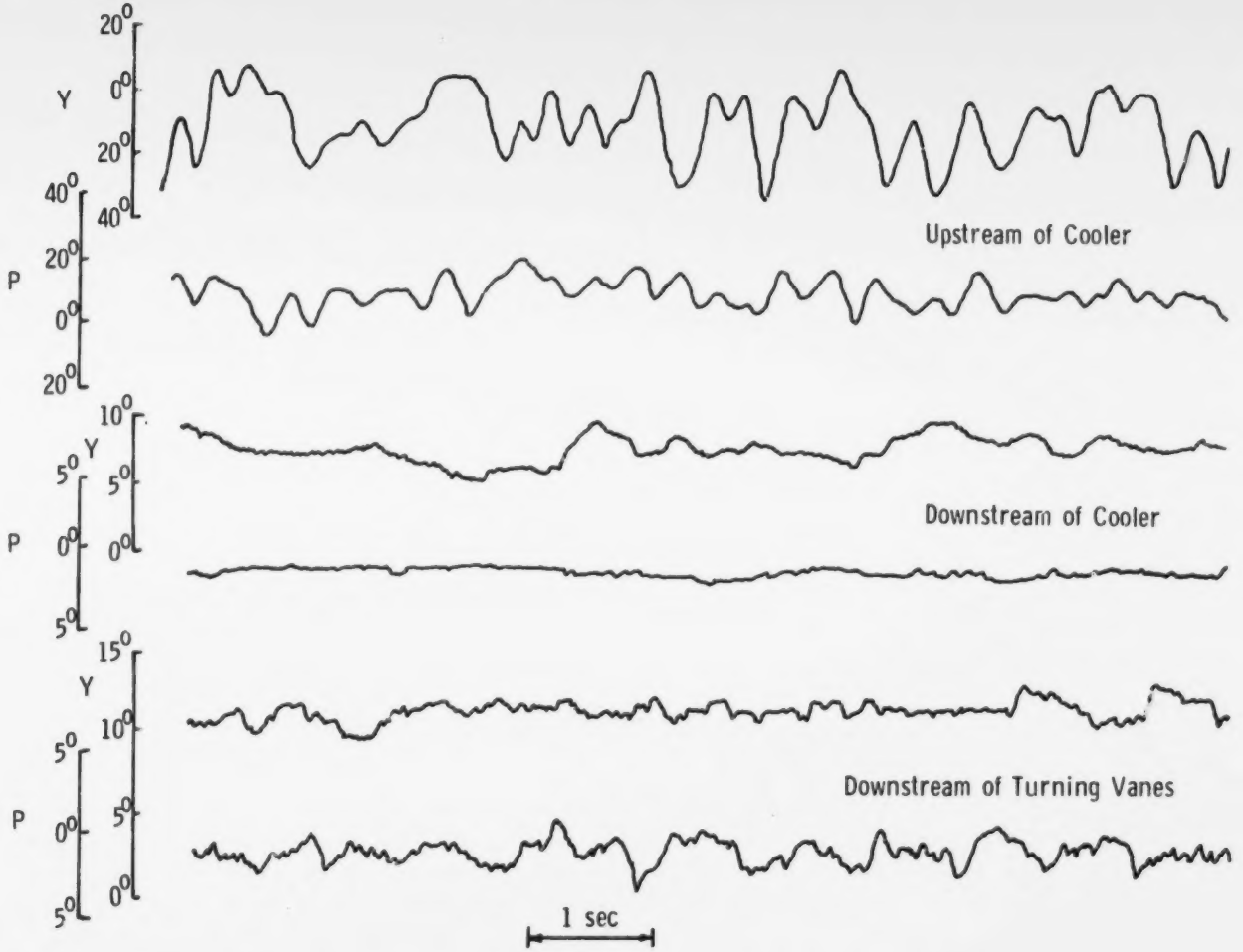

(a) Test-section Mach number of 0.75.

Figure 7.- Time history of flow direction in Langley 8-Foot Transonic Pressure Tunnel.
P = Pitch; Y = Yaw.

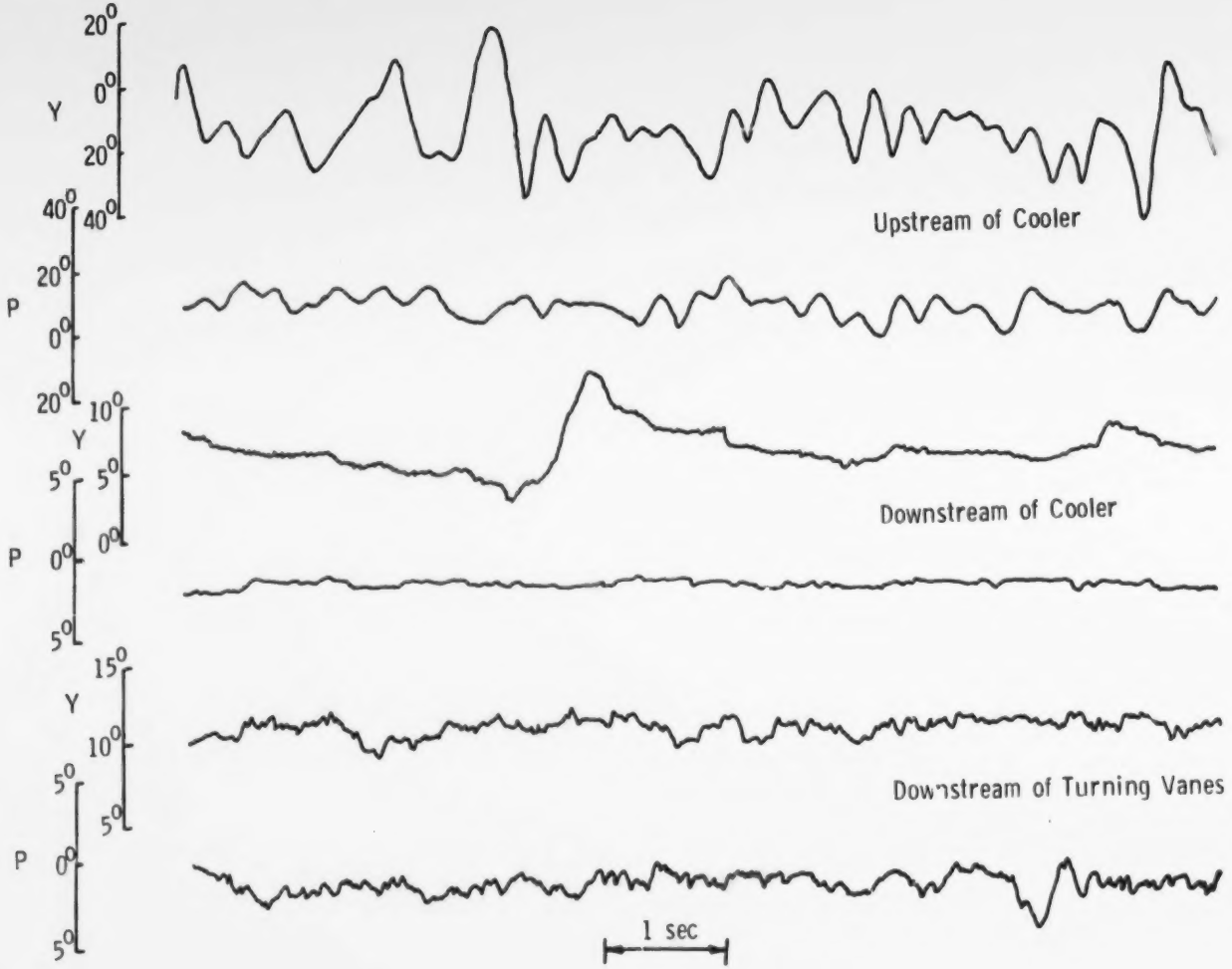

(b) Test-section Mach number of 0.80.

Figure 7.- Continued.

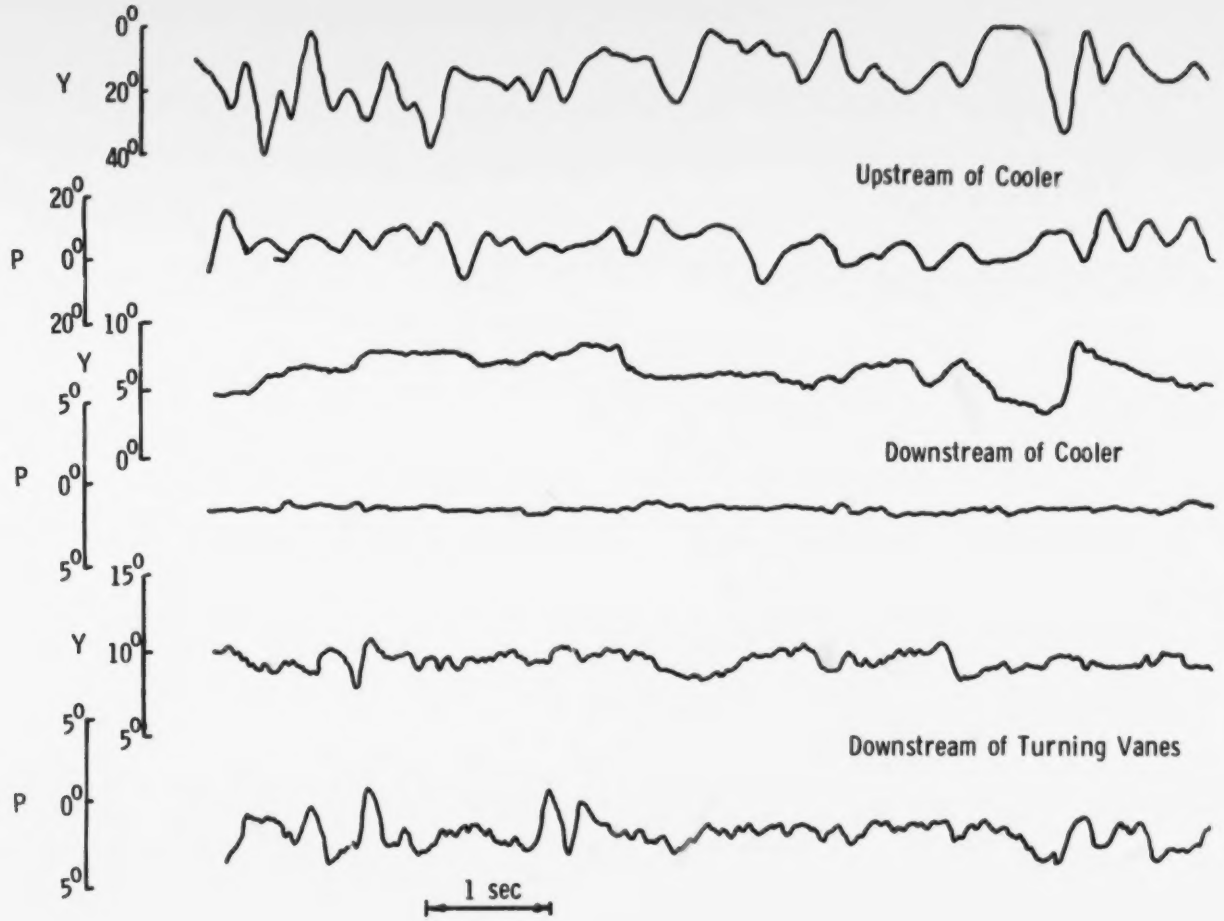

(c) Test-section Mach number of 0.84.

Figure 7.- Concluded.

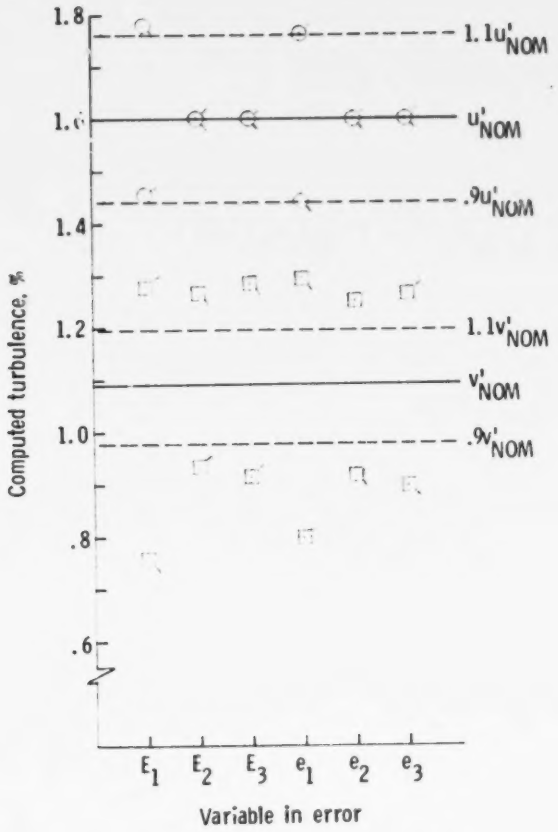

(a) Measured voltage variables.

E_i = dc volts

e_i = rms volts

$$S_{i1} = \frac{\partial \ln E_i}{\partial \ln U}$$

$$S_{i2} = \frac{\partial \ln E_i}{\partial \theta} = L_{i1} U + L_{i2}$$

i = 1 for the single (90°) hot wire

i = 2 or 3 for one of the cross wires

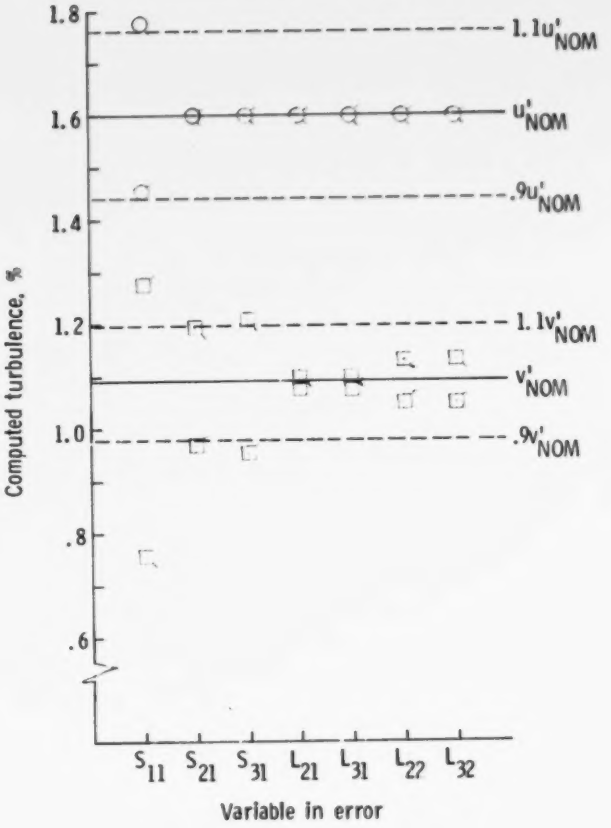

(b) Calibration variables.

Figure 8.- Calculated turbulence using typical input values and introducing ±10 percent error for one variable (indicated on abscissa). Turbulence for u' = O and v' = □. Up flag on symbol corresponds to +10 percent error in one input variable and down flag corresponds to -10 percent error.

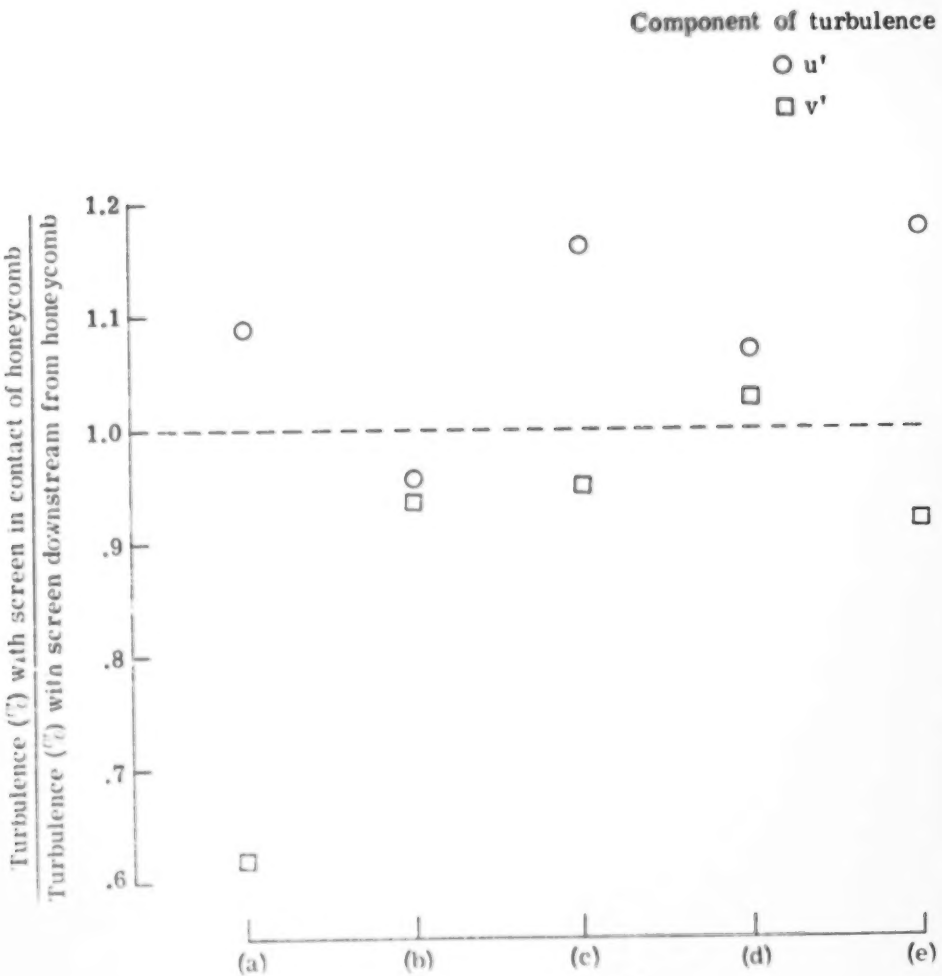

Table VII

Figure 9.- Comparison of screen in contact with downstream edge of honeycomb and same screen downstream of honeycomb trailing edge. Data taken from table VII.

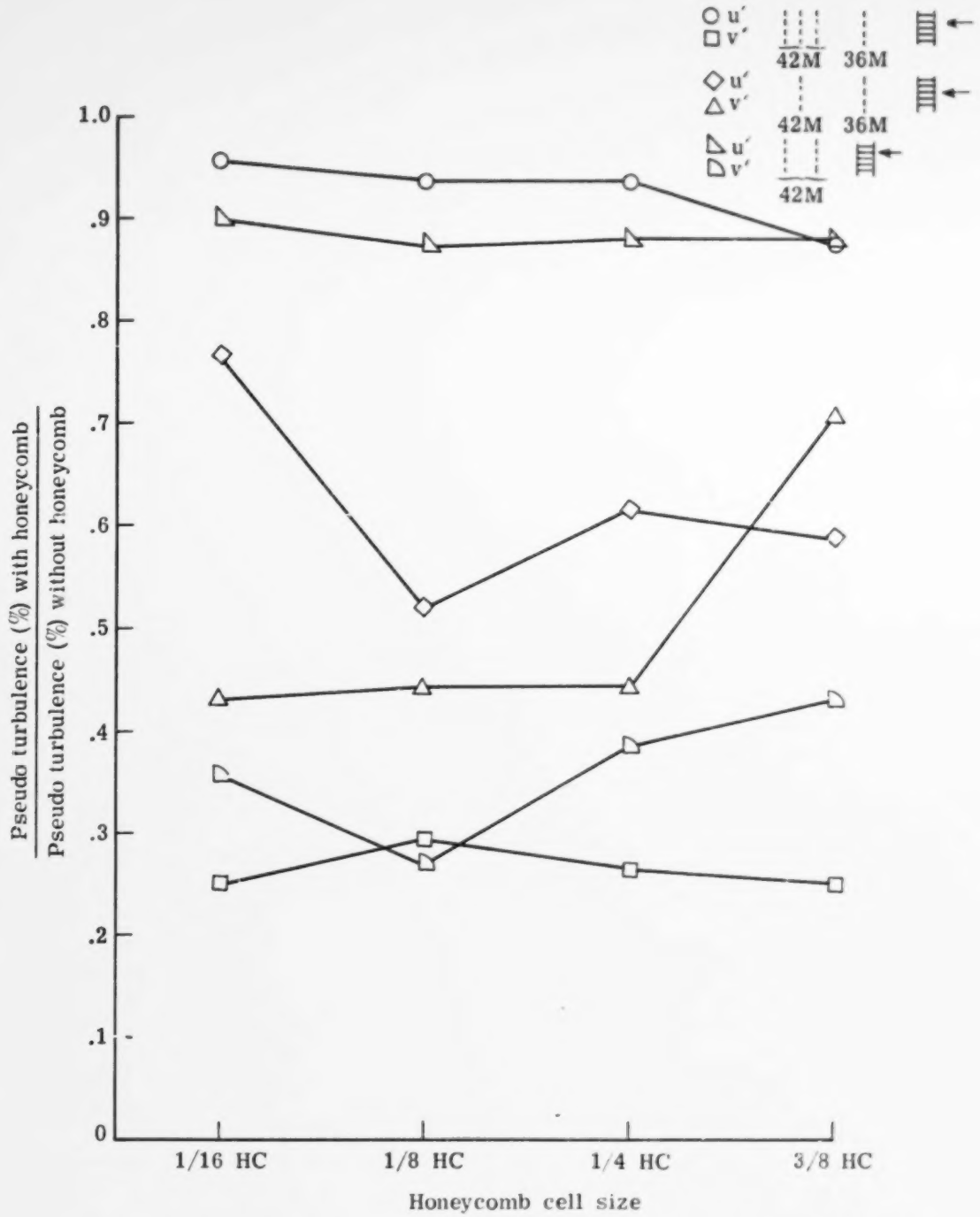

Figure 10.- Evaluation of average (over speed range) turbulence reduction for different honeycomb sizes. Honeycomb cell-length to cell-width ratio between 6 and 8. Data from table IX.

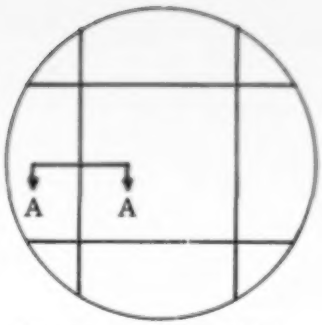

Cross section of full-scale tunnel

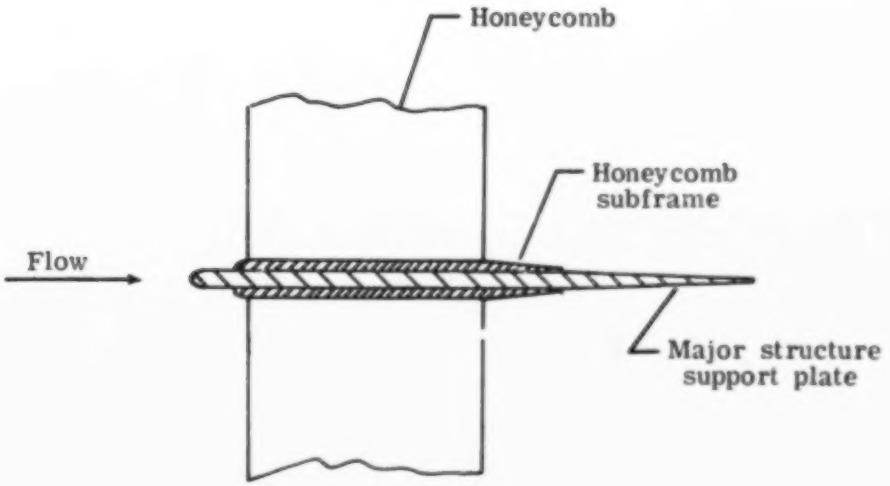

Section A-A

(a) Support configuration A. (See table X(b).)

Figure 11.- Sketch of various honeycomb support techniques investigated. Full-scale wind tunnel is 10.97 m (36 ft) in diameter.

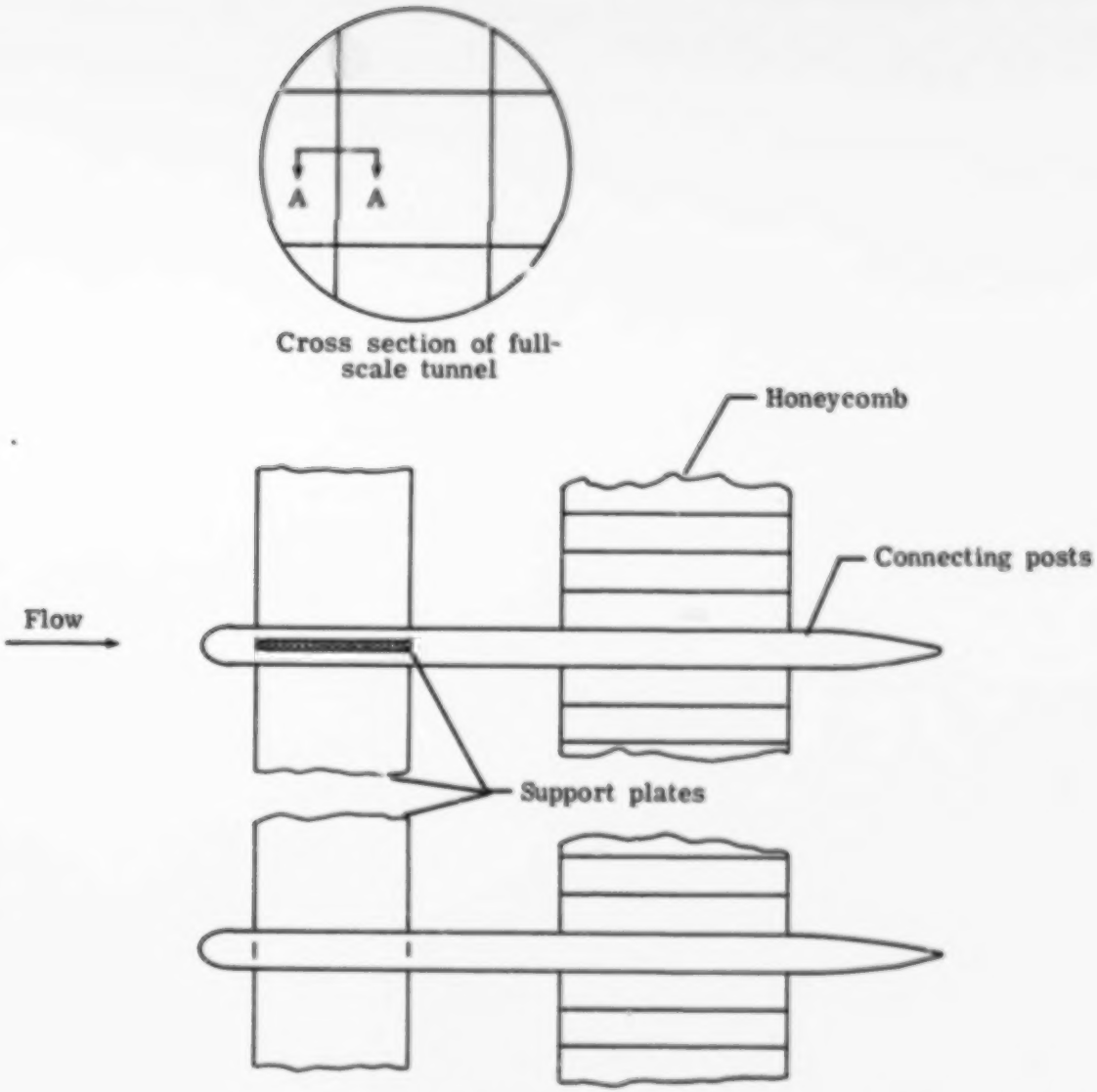

(b) Support configuration B. (See table X(d).)

Figure 11.- Concluded.

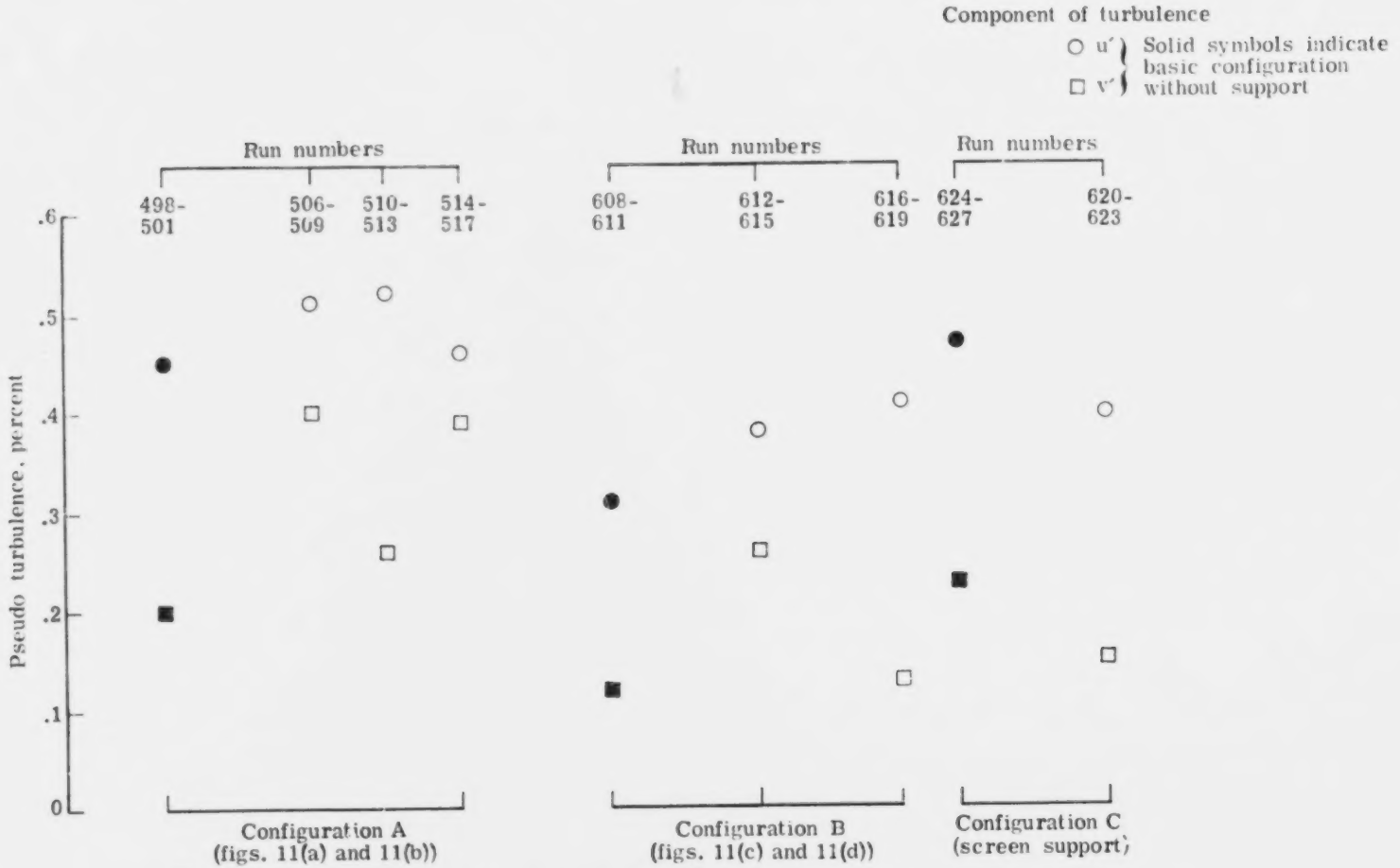

Figure 12.- Evaluation of various techniques for supporting honeycomb in duct.
Data from table X.

1. Report No.	2. Government Accession No.	3. Recipient's Catalog No.
NASA TM-81868		

4. Title and Subtitle	5. Report Date
CONSIDERATIONS FOR THE INSTALLATION OF HONEYCOMB AND SCREENS TO REDUCE WIND-TUNNEL TURBULENCE	August 1981
	6. Performing Organization Code 505-31-43-02
7. Author(s) James Scheiman	8. Performing Organization Report No. L-14109
	10. Work Unit No.
9. Performing Organization Name and Address NASA Langley Research Center Hampton, VA 23665	11. Contract or Grant No.
	13. Type of Report and Period Covered Technical Memorandum
12. Sponsoring Agency Name and Address National Aeronautics and Space Administration Washington, DC 20546	14. Sponsoring Agency Code

15. Supplementary Notes

16. Abstract

Tests were conducted on a half-scale model representing a 0.914-m (3.0-ft) square stream tube of the flow through the fourth corner and settling chamber of the Langley 8-Foot Transonic Pressure Tunnel. The model included the finned-tube cooler, 45° turning vanes, and the turbulence reduction screens and honeycomb, which were the subject of the tests. Hot-wire measurements of the turbulence reduction for various combinations of screens and honeycomb were made at various duct speeds. Of the four sizes of honeycomb cells tested, none were found to have a superior performance advantage. The effectiveness of screens and honeycomb in reducing turbulence is greatly affected by relatively minor physical damage; therefore, extreme care must be exercised in installing and maintaining honeycomb or screens if the turbulence reduction performance is to be maintained.

17. Key Words (Suggested by Author(s))

Turbulence reduction
Wind tunnel
Screens
Honeycomb

18. Distribution Statement

Unclassified - Unlimited

Subject Category 09

19. Security Classif. (of this report)	20. Security Classif. (of this page)	21. No. of Pages	22. Price
Unclassified	Unclassified	51	A04

For sale by the National Technical Information Service, Springfield, Virginia 22161

NASA-Langley, 1981